



# **Mountain Home Geothermal Area: Natural State Model**

**Sabodh K. Garg**

**Technical Report**

**Leidos, Inc.  
10260 Campus Point Drive  
San Diego, CA 92121**

**Submitted to:  
Utah State University  
4505 Old Main Hill  
Logan, Utah 84322**

**May 2017**

## I. Background

Under a co-operative agreement with the U.S. Department of Energy (DOE), Utah State University is carrying out a research program to identify promising geothermal prospects in the Snake River Plain (SRP) volcanic province. The goals of this study are to: (1) adapt the methodology of *Play Fairway Analysis* for geothermal exploration, creating a formal basis for its application to geothermal systems, (2) assemble relevant data for the Snake River Plain volcanic province from publicly available and private sources, and (3) build a geothermal play fairway model for the Snake River Plain that will allow the delineation of the most promising plays. The model will serve to integrate the diverse data sets and serve as a point of departure for future exploration efforts in the region. A promising play type is associated with the SRP basaltic sill-complexes characterized by fault-controlled permeability, volcanic sill heat source, and lake sediment seal. The area around Mountain Home Air Force base in western Snake River Plain (Figure 1) hosts a geothermal system of the latter type.

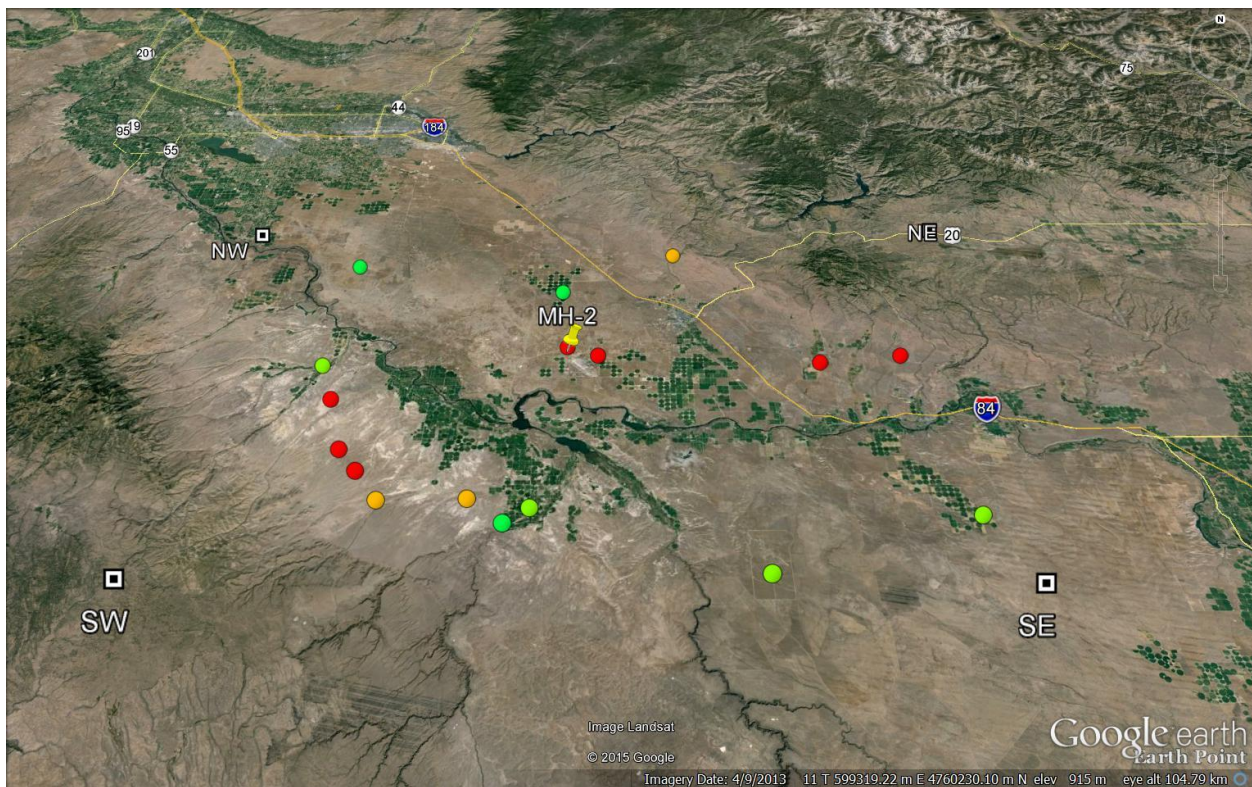


Figure 1: Mountain Home area showing the locations of boreholes greater than 200 meters in depth. The NW (Lat: 43.31, Long: -116.51), NE (43.31, -115.19), SW (42.71, -116.50), and SE (42.71, -115.20) denote the four corners of the area.

The Mountain Home area is characterized by high heat flow and temperature gradient. Temperature data are available from 18 boreholes (Figure 1) with depths equal to or greater than 200 m; although there are large variations, the average temperature gradient exceeds 80°C/km. In a previous report, the author (Garg, 2015) presented a preliminary 3-D numerical model of the natural-state (i.e. pre-production state) of the Mountain Home geothermal area shown in Figure 1; the latter model was conditioned using the available temperature profiles from the five deep wells with depths ranging from ~1340 m to ~3390 m (MH-1, MH-2, Bostic1, Lawrence D No.1, and Anschutz No. 1). Recently, high resolution gravity, ground magnetic, magnetotelluric (MT), and seismic reflection surveys have been carried out in the area in order to define key structural features responsible for promoting permeability and fluid flow (Glen et al., 2017). Of particular relevance is the MT survey performed in the Mountain Home area (see Figures 2a and 2b for MT station locations).

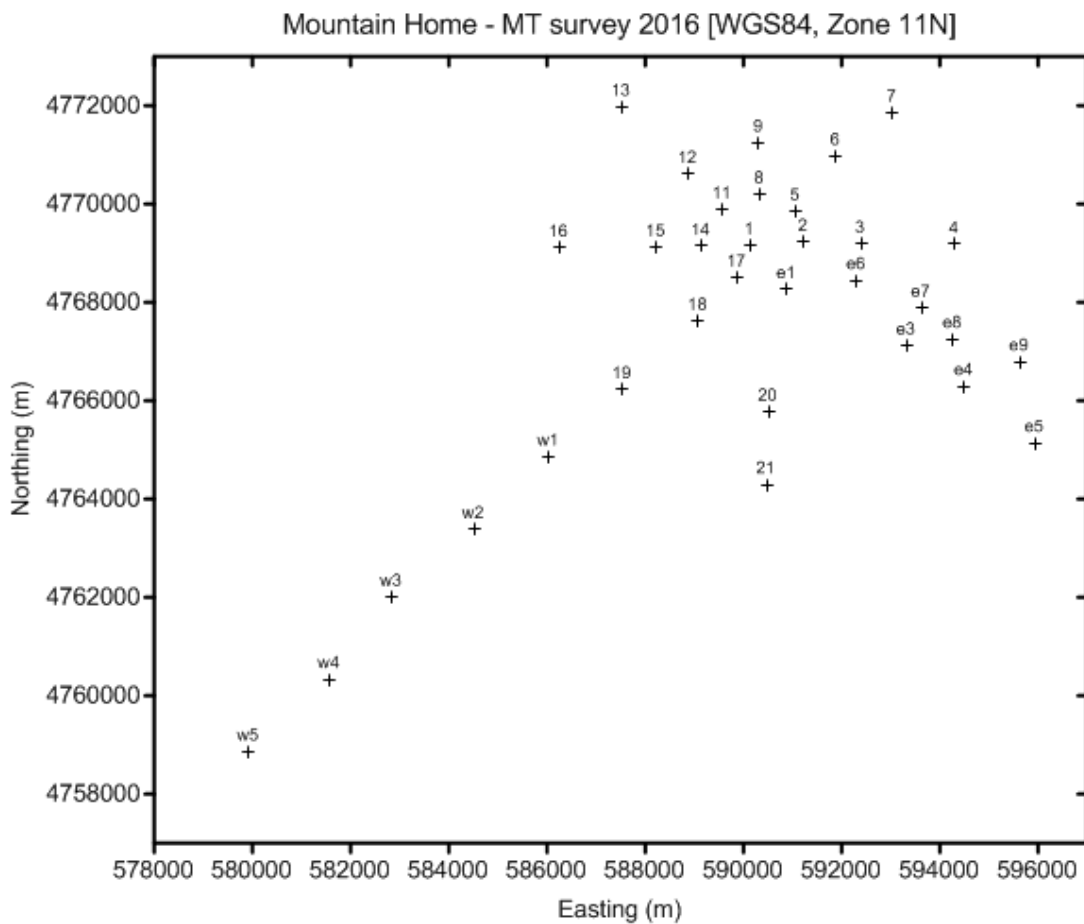


Figure 2a: MT station locations (figure provided by Erika Gasperikova). 3D resistivity distribution from MT inversion is shown in Figure 3a and recovered resistivity variations along a SW-NE profile as a function of depth extending from station w2 to 7 is shown in Figure 3b.

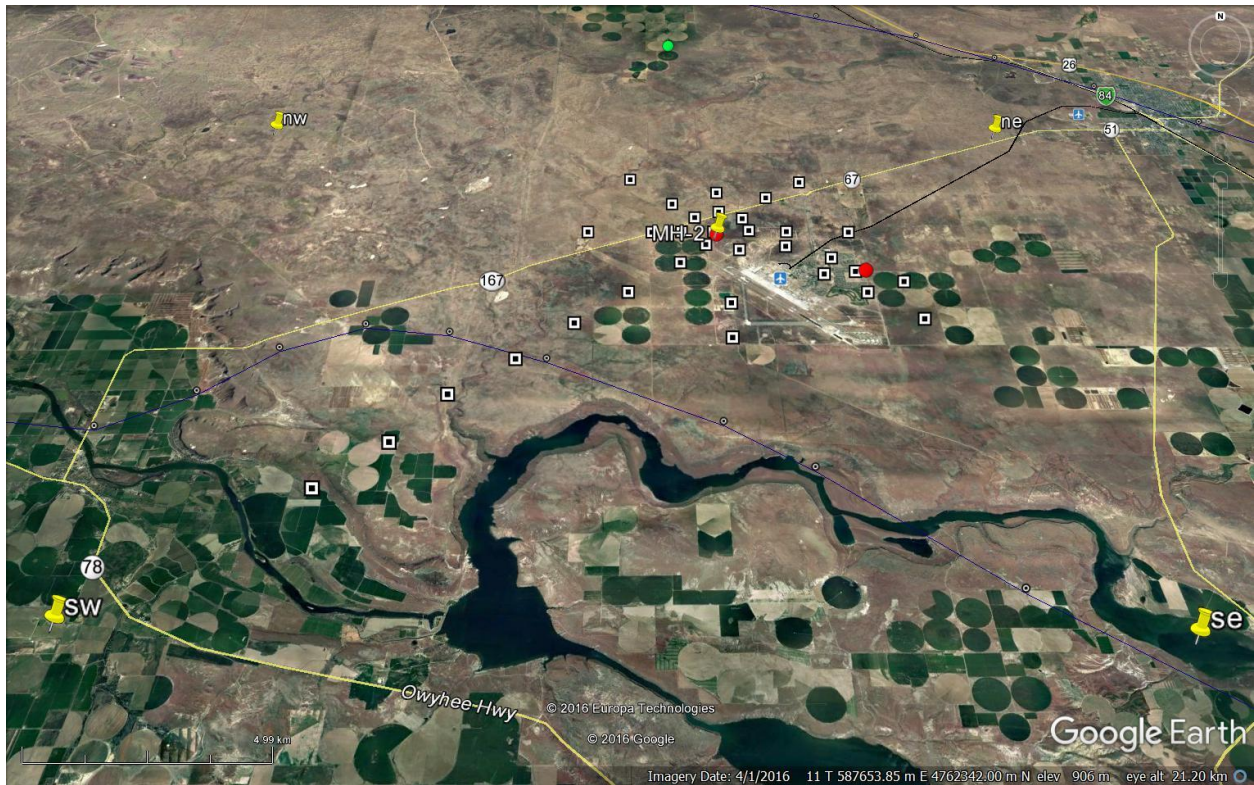


Figure 2b: Mountain Home area showing the locations of boreholes MH-1 and MH-2 (red circles) and MT stations (white rectangles). The blue line passing to the north of station w2 denotes a deep gravity fault. The NW (Lat: 43.1240, Long: -116.0780), NE (43.1211, -115.7707), SW (42.9439, -116.0807), and SE (42.9411, -115.7743) denote the four corners of the area (25 km by 20 km) used for the numerical model described below; note that the latter area is only about 6% of the area shown in Figure 1.

MT data acquired around the MH-2 well were used for 3D MT inversion. The study area included in this inversion was  $\sim 13 \times 10$  km. There is a gap in data coverage SE and E of the MH-2 well (between MHE1 and MHE3 and MHE1 and MH04): due to the Air Force Base (AFB) cultural noise the data at those stations were not usable for interpretation. The final resistivity structure recovered by 3D MT inversion is shown in Figure 3a (Gasperikova, personal communication, 2017). Low resistivity (1-10 Ohm-m) distribution in 3D resistivity cube outlines the lateral and depth extent of what would be considered a seal structure for a potential geothermal reservoir. This structure would presumably have a low permeability. The uppermost resistive layer (200-500 Ohm-m) is representative of near surface unaltered porous basalts, while increased resistivity ( $>40$  Ohm-m) underneath the low resistivity structure is representative of volcanic formations that could be associated with production of geothermal fluids. Figure 3b shows SW-NE resistivity cross-section extracted from 3D resistivity model with a gravity inversion model superimposed in black. The gravity profile is 3 km to SE and runs parallel to this profile. There is a very good agreement between resistivity and gravity interpretation. Similar structures were recovered on the Eastern side of the basin, close to Bostic well (Figure 3c), using MT data collected in 1980 by Unocal. Again, MT and gravity interpretations agree well at that location.

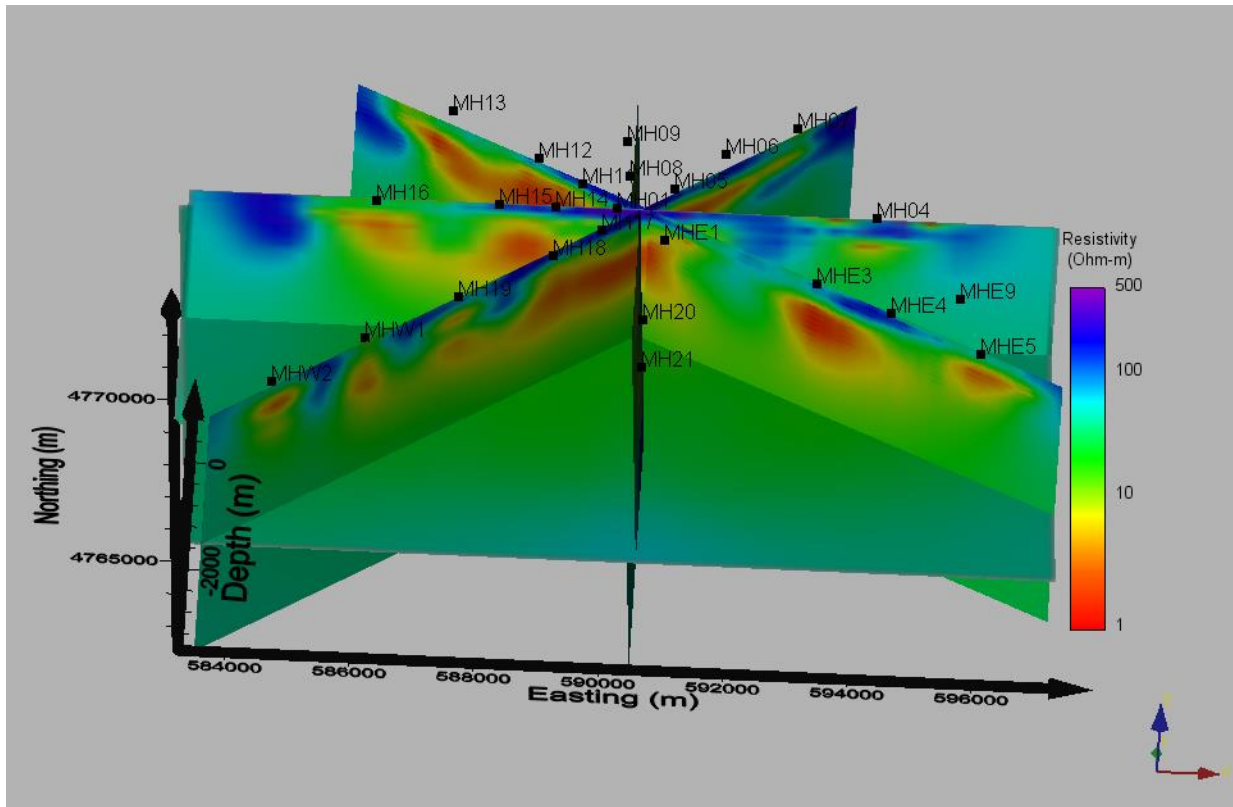


Figure 3a: 3D resistivity model

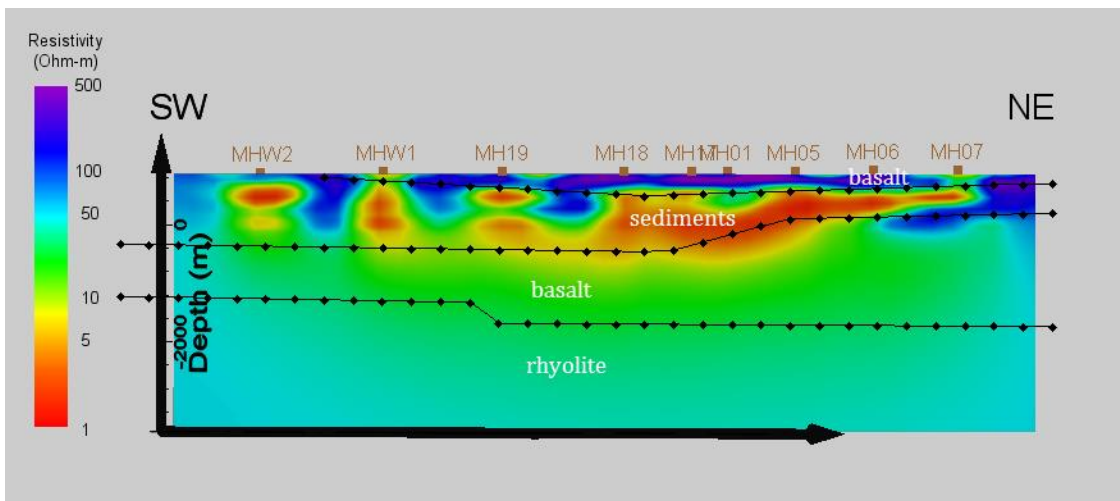


Figure 3b: SW-NE resistivity cross-section extracted from 3D resistivity model. Black lines with diamonds indicate unit interfaces (white labels) from gravity inversion along a profile 3 km SE of this profile.

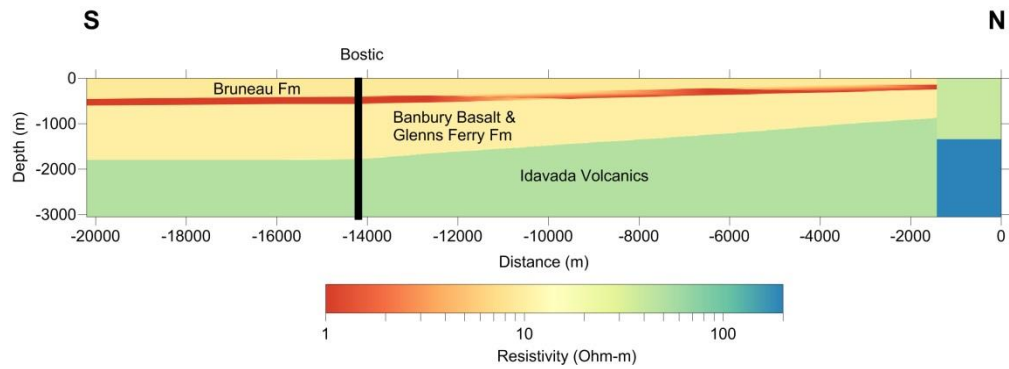


Figure 3c: 2D resistivity cross-section at Bostic based on Unocal 1980 MT data. The profile location is shown in Figure 3d; Distance 0 m is ~1 km North of station 14, and -20,000 m is ~1 km South of station 54.

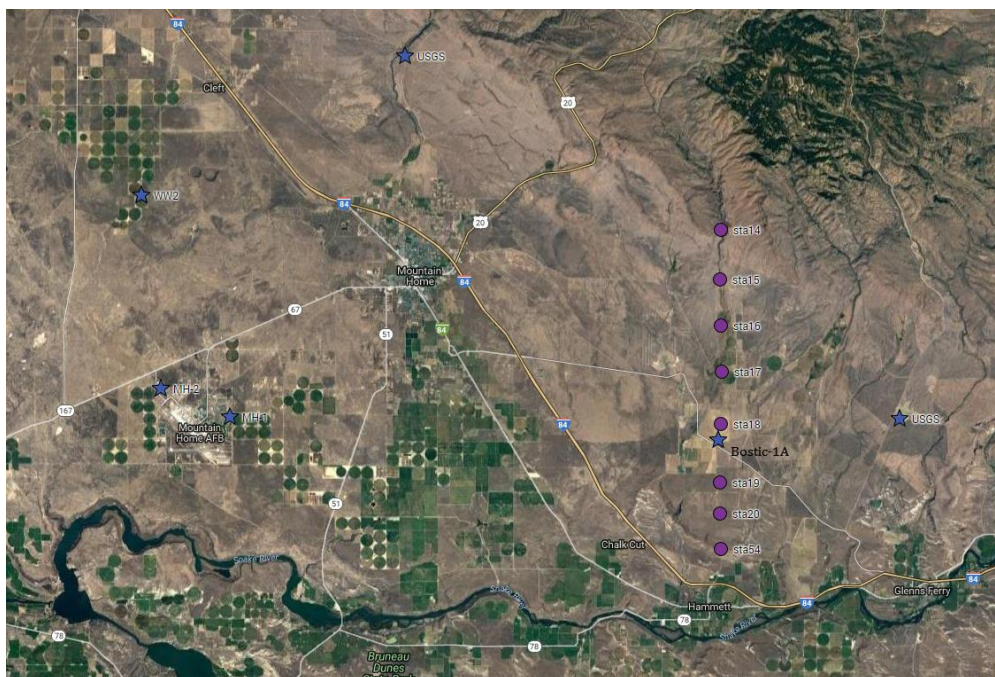


Figure 3d: Location of the profile shown in Figure 3c.

The above interpretation of MT data forms the basis of the numerical reservoir model presented in the following sections.

## Numerical Model – an Introduction

A hydrothermal system such as the Mountain Home geothermal prospect contains a convecting fluid mixture that is heated at depth and then rises towards the surface as a consequence of buoyancy. The system is not only nonisothermal but is also in a continuous state of flow.

The development of a natural-state model requires a variety of geological, geophysical, geochemical and hydrological data sets. A computer based simulation of the natural fluid and heat flow in the geothermal reservoir offers the framework for synthesizing these evolving data sets (*i.e.*, presumably as a result of drilling and production/injection operations) into an integrated geohydrological model. Such natural-state modeling also helps in the evolution of the conceptual model by revealing inconsistencies and physical shortcomings in the preliminary conceptual model of the reservoir.

Assessment of the natural-state model is usually carried out by comparing theoretical predictions of quantities such as reservoir pressure and temperature, and surface heat and mass discharge with field measurements. This process very often provides insight into reservoir parameters such as formation permeability distribution, and boundary conditions for heat and mass recharge at depth. The natural-state model can also be used to evaluate the effects of gaps in the available data base on future reservoir performance. Planning of future drilling and well tests for reservoir verification could then be based on resolving major uncertainties in the evolving model for the geothermal reservoir. For fields which have not yet been exploited, or have been in operation for only a few years, the natural-state information comprises the bulk of the data available for reservoir modeling.

It is not sufficient to merely prescribe a “natural state” based, for example, upon interpolation between measured, or inferred, pressures and temperatures. It is essential, in fact, that the natural state itself represents a quasi-steady solution of the partial differential equations that govern flow in the reservoir. Otherwise, solution of the production/injection phase of the problem is likely to produce changes in underground pressures and temperatures that are unrelated to exploitation, but are instead fictitious consequences of the initial (*i.e.*, pre-production or natural) conditions being inconsistent with steady behavior. Since transient processes associated with initiation of convection occur over time scales of the order of  $10^4$  to  $10^5$  years, the natural state can be regarded as stationary over the 10–50 year period required to exploit a geothermal reservoir. Thus, the requirement that the natural state be itself a nearly steady solution of the governing equations is an essential test of the model of the reservoir.

A definite volume must be chosen for a computer simulation of the reservoir system. For modeling purposes, it is useful to visualize the reservoir as a region of hot water surrounded by cold water on the sides. The reservoir boundaries are usually diffuse and irregular because of variations in formation properties such as permeability; for the sake of simplicity, the boundaries are assumed to have simple geometrical shapes. At the margins of the field, there are inflows of cold water and outflows of hot water and the temperature pattern is complicated. Inside the reservoir itself, cold- water recharge from the top and/or sides will mix with the hot water inflow from the base and produce spatial variations in the fluid state.

Determination of the natural state amounts to solving an inverse problem, and is accomplished by a procedure amounting to successive approximation. The quasi-steady (or stationary) state depends mainly upon the boundary conditions imposed upon the perimeter of the system volume (such as pressures, temperatures, and deep heat flux and hot fluid sources) and upon the distributions of formation properties (such as porosity and permeability) believed to prevail within it. Thus, given estimates of the boundary conditions and formation properties, the

corresponding stable state is found. This solution may be examined to see how well it matches known facts about the system (such as measured downhole pressures, temperatures, fluid state, advective zones within the reservoir and distribution of surface discharge). Appropriate adjustments are then made in the boundary conditions and/or formation properties in an effort to improve agreement between measurements and computed results, and the problem is solved again. In this way, the natural state is found in an iterative fashion involving repetitive calculations of the pseudo-steady state.

The pseudo-steady states are usually computed by carrying out a time-dependent calculation representing thousands of years of physical evolution of the reservoir. A fundamental conceptual problem exists in the selection of the boundary conditions and the initial conditions. During the thousands of years required for the evolution of the reservoir to its present state, the boundary conditions themselves must have undergone change. Thus, for example, heat transfer from a magma intrusion is at a maximum just after its emplacement, and declines (exponentially?) with time. We have, of course, no way of determining the evolution of boundary conditions with time, and must perforce employ time invariant boundary conditions. These time invariant boundary conditions are usually chosen to represent the present day situation. The time dependent calculation does not, therefore, strictly represent the actual physical evolution of the system; it is rather an attempt to mimic the evolution of the geothermal system to its present state using a mathematically tractable model. As far as the specification of initial conditions is concerned, the problem is somewhat simpler. The influence of the initial conditions upon the solution declines as time goes on and, in principle, becomes exactly zero when a steady state is reached. Therefore, the exact details of the initial conditions are relatively unimportant. All that is required for initial conditions is a state that is (1) physically plausible and (2) consistent with the applied boundary conditions.

Despite the fact that (as noted above) the calculation of the evolution of the system to the natural state does not exactly replicate the true evolution over time due to the necessity of imposing constant boundary conditions and fixed formation property distributions and to uncertainties concerning the exact initial state, the time-duration of the natural-state calculation should bear some resemblance to reality. The typical ages of geothermal systems vary from  $\sim 10^4$  to  $\sim 10^6$  years, but in tectonically active volcanic regions such systems are unlikely to remain unchanged for over  $\sim 10^5$  years or so. This means that the system will never reach an exactly steady condition since the time required for thermal conduction processes (the slowest heat transfer mechanism) to reach equilibrium will normally be much longer. Generally speaking, natural-state calculations usually represent between  $10^4$  and  $10^6$  years; the resulting state, while not exactly steady, will be characterized by changes that are imperceptible on time-scales of centuries. As such, they comprise appropriate starting conditions for modeling reservoir exploitation.

## **II. Computational Volume, Model Grid, Formation Properties, and Boundary Conditions**

The ground surface elevation in the Mountain Home area (Figure 2a) varies from about 700 mASL (meters above sea-level) to  $\sim 1000$  mASL. The MT survey indicates the presence of

permeability to a depth of about 5000 meters below sea-level (Figure 3). The bottom of the model grid is placed at 4500 m below sea-level; thus the model grid covers essentially all of the permeable volume. The top of the model grid is at the assumed water level (1 bar surface).

At present, no pressure transient data are available from any of the wells in the Mountain Home area. The vertical permeability values were determined during the development of the numerical model in order to match the measured well temperatures. The horizontal permeability values in the model are largely unconstrained. In the future, permeability values used in the model will be modified as additional geological, geophysical, and well test data become available.

The model volume is divided into a 25x20x25 grid in the x- and y- and z-directions (east, north, and vertically upwards) respectively. In the z-direction, the grid blocks are either 100 m or 250 m. In the x- and y-directions, a uniform grid spacing of 1 km was employed. The total number of the grid blocks is 12,500, and the model volume is 2750 cubic kilometers (25 km in the east-west direction, 20 km in the north-south direction, and 5.5 km in the vertical direction). An overlay of the horizontal grid over the Mountain Home area is shown in Figure 4. The vertical grid is displayed in Figure 5.

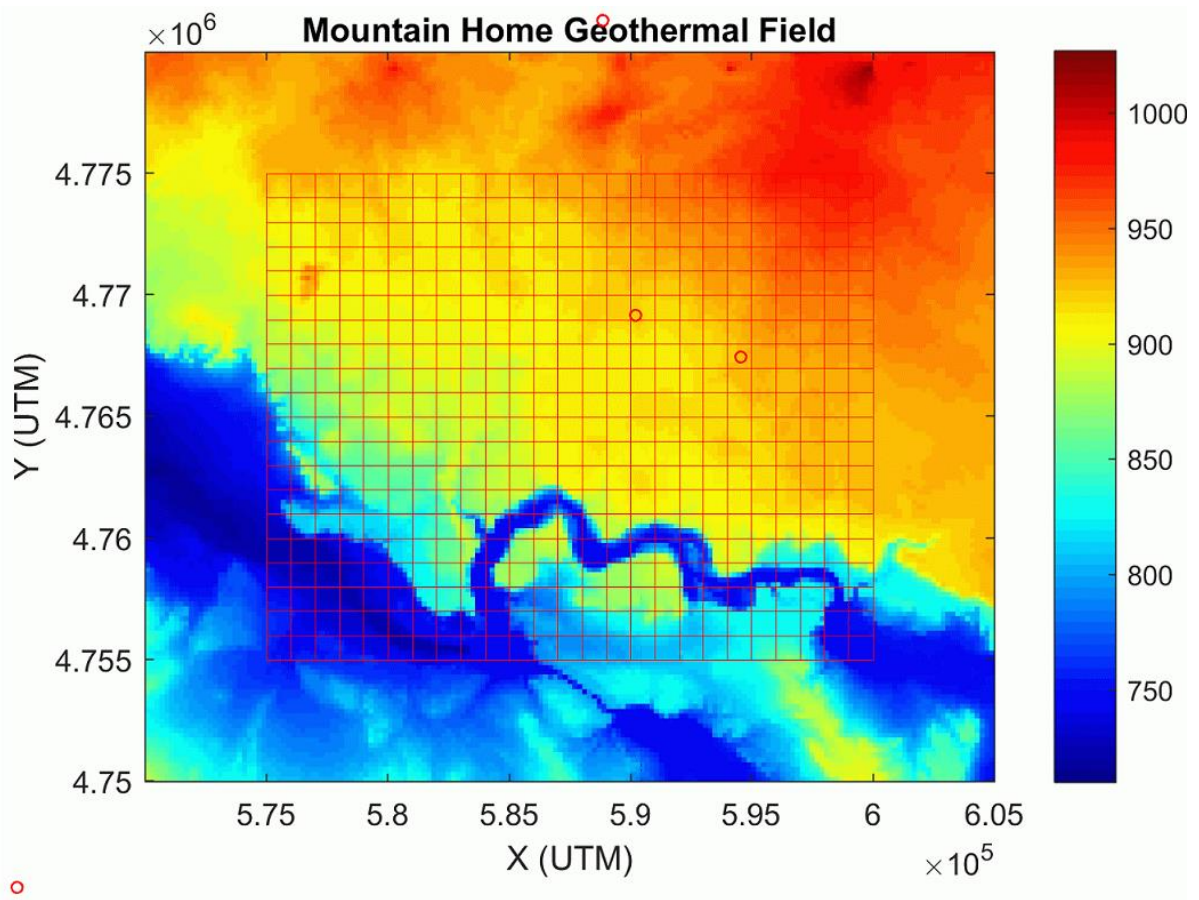


Figure 4: Horizontal grid (x-y grid) superposed on a topographic map of the Mountain Home area; warm colors denote higher elevations. Well-heads (red

circles) are also shown. The origin of the model grid is at 575,000 mE and 4,755,000 mN (UTM).

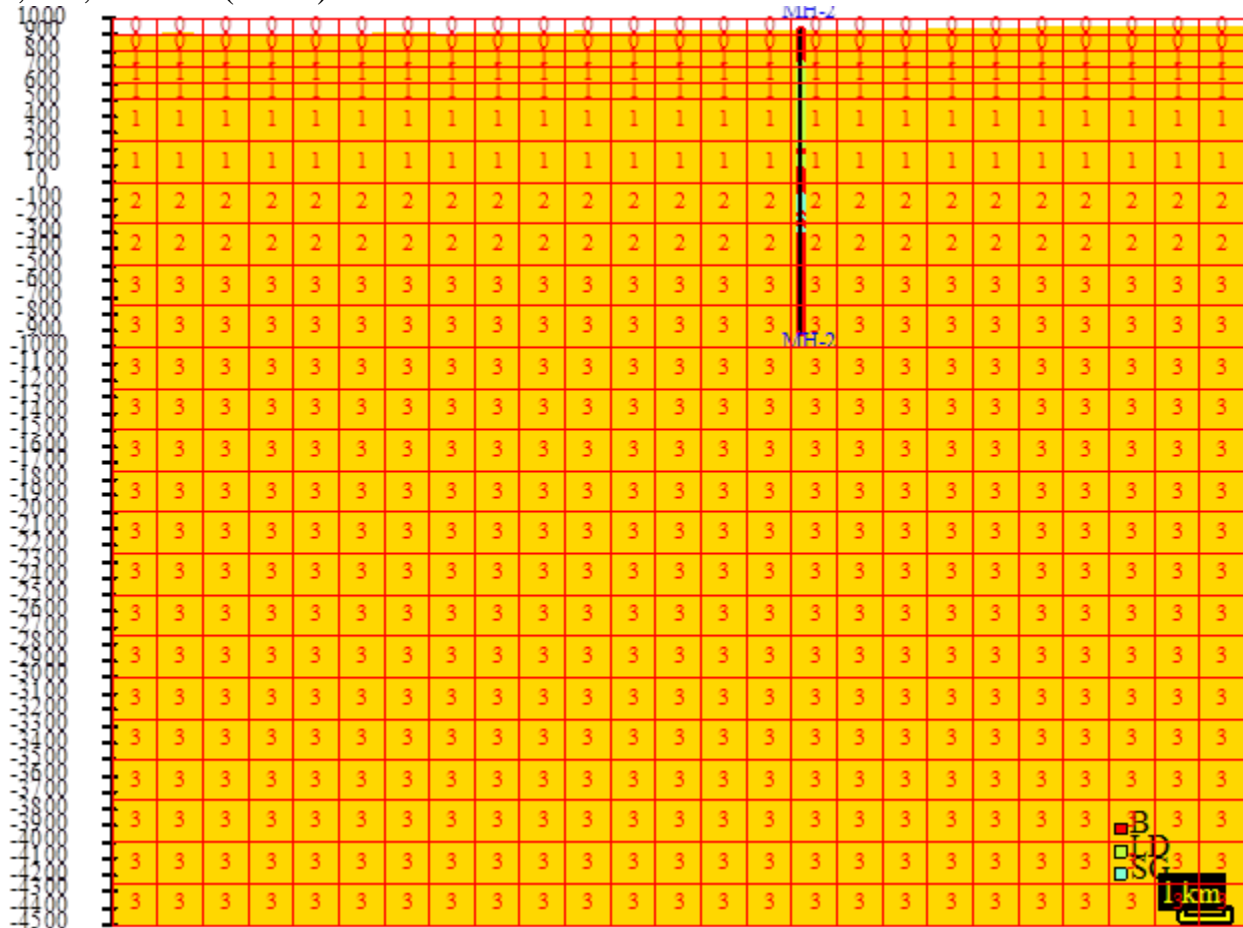


Figure 5: Vertical (x-z) model grid at  $y= 14.5$  km ( $j=15$ ). The bottom of the grid is at -4500 mASL. The bottom 20 grid blocks ( $k=1$  to 20) are of uniform thickness (250 m each); a smaller thickness (100 m) is used for blocks  $k=21$  and higher in order to more closely represent the water level surface. Numbers in grid-blocks (1, 2, 3, and 4) denote the formation type (see below). The void blocks are tagged with 0. Also shown is the lithology from the deep well MH-2 passing through  $j=15$ .

The 3-D numerical model was constructed using Leidos’s STAR geothermal reservoir simulator (Pritchett, 2011). In order to carry out model computations with STAR (or for that matter any other reservoir simulator), it is essential to prescribe distribution of thermo-hydraulic properties (*e.g.*, permeability, porosity, thermal conductivity, specific heat, etc.) for the entire grid-volume, and boundary conditions along the faces of the model grid. During the development of the natural-state model for the Mountain Home geothermal prospect presented below, the boundary conditions (*i.e.*, heat flux along the bottom boundary, pressure specification along the top boundary) and the formation permeabilities were freely varied in order to match the observed temperature profiles in wells. Several such calculations were carried out; in the following, we will only describe the final case.

Formation properties utilized for the Mountain Home natural-state model are given in Table 1. Distribution of the formation properties within the model grid is shown in Figures 6a to 6u. Rock types assigned to individual grid blocks (Figures 6a-u) are in part based on lithological logs from wells MH-1 and MH-2. The average vertical permeability at Mountain Home appears to be rather low. More specifically, a low vertical permeability is required for matching the mostly conductive temperature profiles recorded in wells MH-1 and MH-2. As mentioned previously, the assumed horizontal permeabilities are essentially arbitrary, and are unconstrained at the present time.

In addition to formation properties given in table 1, it is necessary to specify capillary pressure and relative permeabilities. The capillary pressure is assumed to be negligible. Straight-line relative permeability curves with a liquid (gas) residual saturation of 0.2 (0.0) are used. Since two-phase flow is unlikely in the “natural state” at Mountain Home, the capillary pressure and relative permeability have no effect on the computed natural-state.

**Table 1: Formation properties.**

Formation Name	Intrinsic rock density (kg/m <sup>3</sup> )	Rock grain specific heat (J/kg-°C)	Global Thermal Conductivity (W/m-°C)	Porosity	Permeability in x-direction (mdarcy)*	Permeability in y-direction (mdarcy)*	Permeability in z-direction (mdarcy)*
1.Sediments/basalt	2800	1000	1.5	0.100	1	1	0.01
2.Basalt upper	2800	1000	1.5	0.025	1	1	0.0135
3.Basalt Lower	2800	1000	1.5	0.025	10	10	1
4.Rhyolite/basalt	2800	1000	1.5	0.025	1	1	0.1

\*It is assumed here that 1 millidarcy is exactly equal to 10<sup>-15</sup> m<sup>2</sup>

**KEY TO "STAR" PLOTS OF UNDERGROUND EARTH STRUCTURE**

- |   |                     |   |                    |
|---|---------------------|---|--------------------|
|  | 1. Sediments/basalt |  | 2. Basalt Upper    |
|  | 3. Basalt Lower     |  | 4. Rhyolite/basalt |

Figure 6a: Key to earth structure; see table 1 for formation properties.

Underground earth structure in x-z plane at "j" = 1 (y = 5.00000E+02 meters).

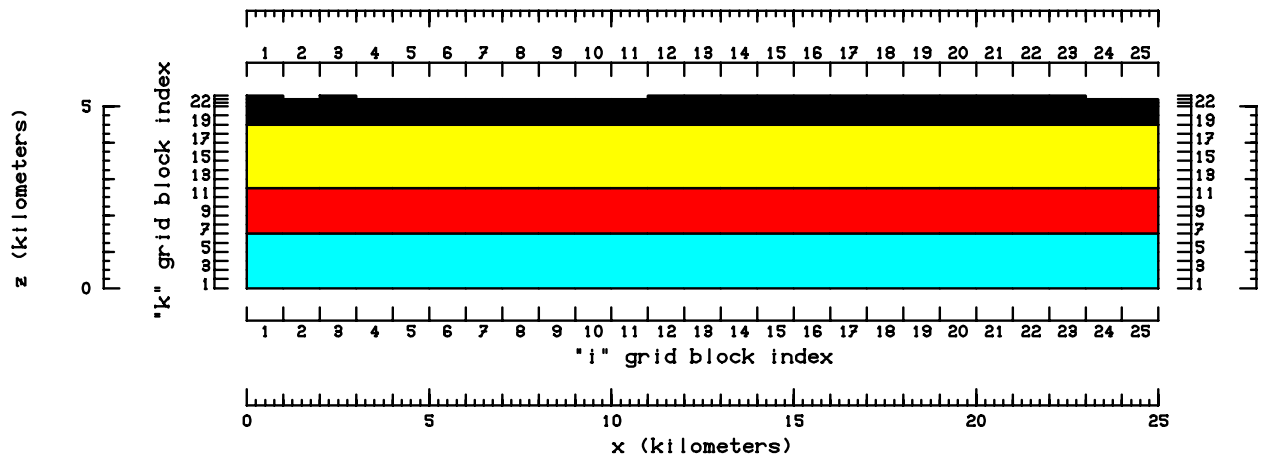


Figure 6b: Earth structure in x-z plane (j=1).

Underground earth structure in x-z plane at "j" = 2 (y = 1.50000E+03 meters).

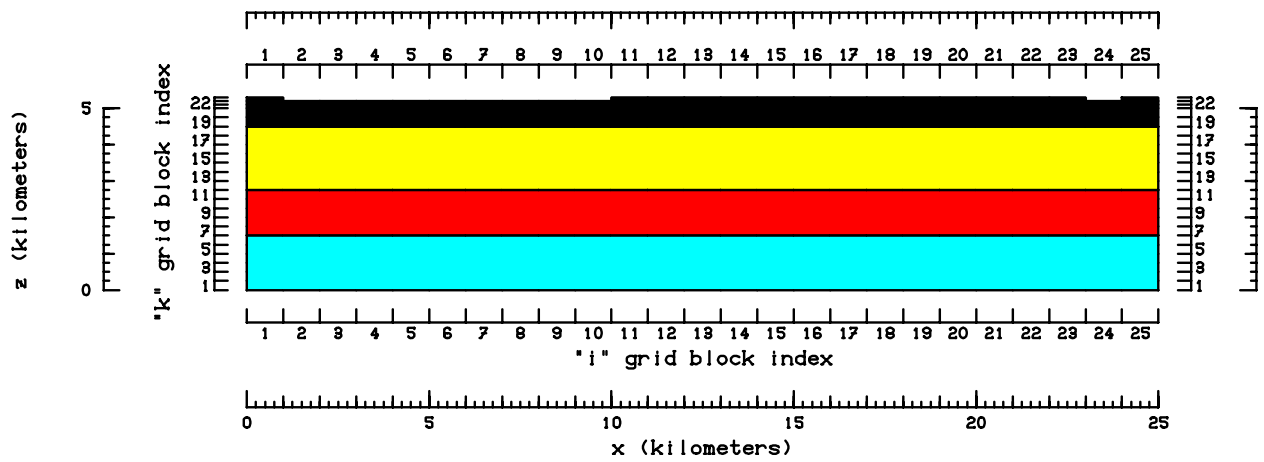


Figure 6c: Earth structure in x-z plane (j=2).

Underground earth structure in x-z plane at "j" = 3 (y = 2.50000E+03 meters).

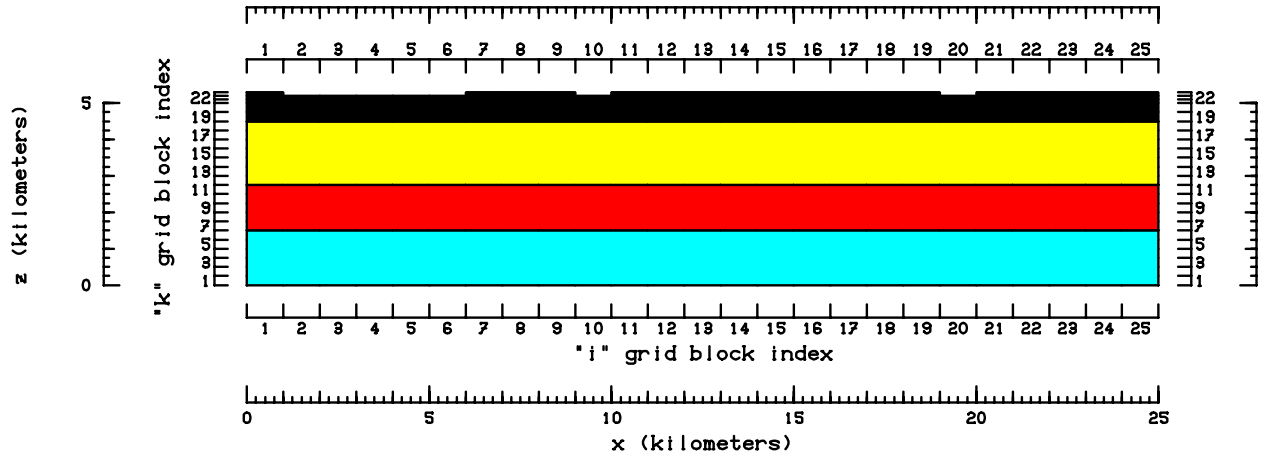


Figure 6d: Earth structure in x-z plane (j=3).

Underground earth structure in x-z plane at "j" = 4 (y = 3.50000E+03 meters).

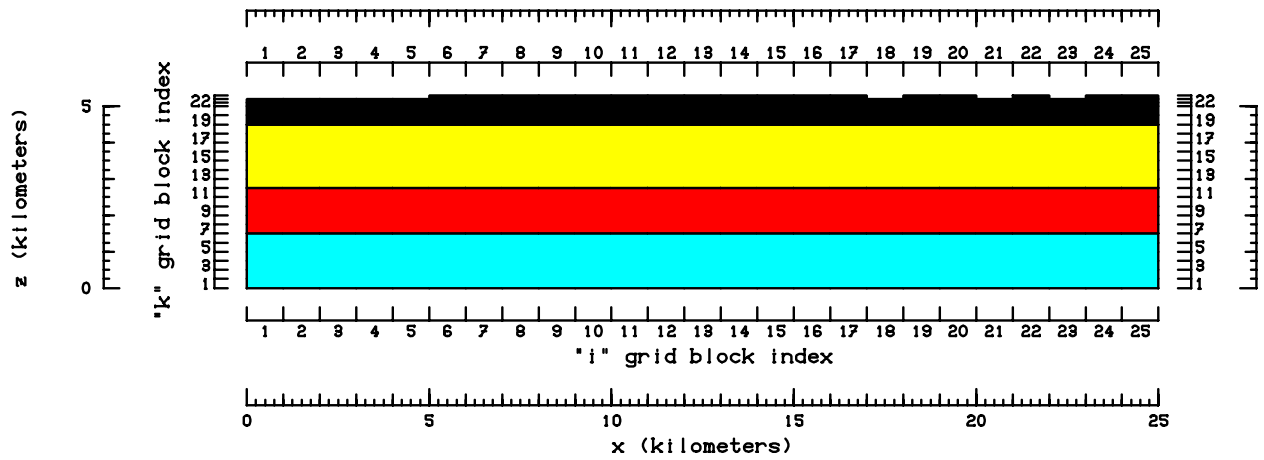


Figure 6e: Earth structure in x-z plane (j=4)

Underground earth structure in x-z plane at "j" = 5 (y = 4.50000E+03 meters).

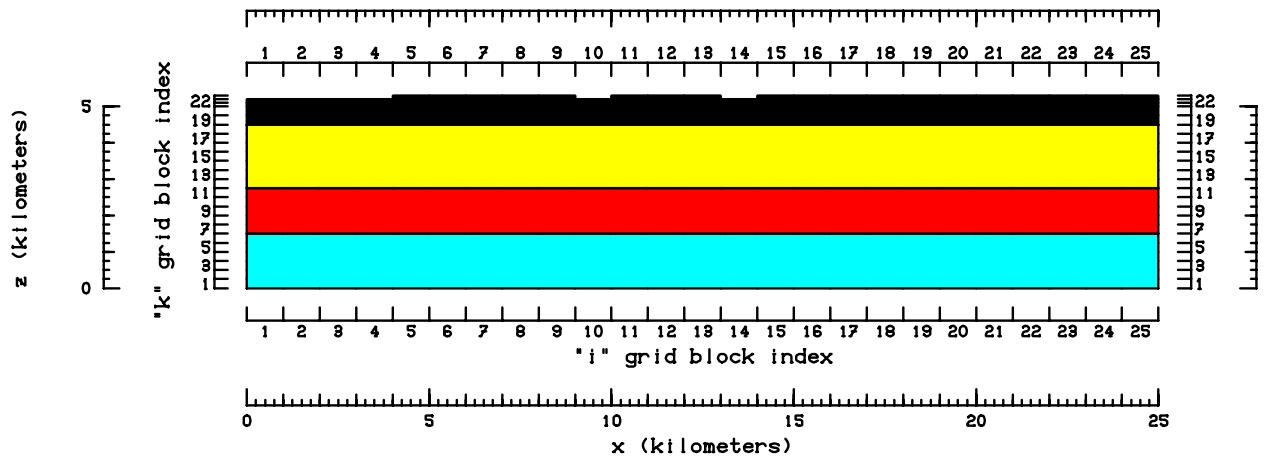


Figure 6f: Earth structure in x-z plane (j=5).

Underground earth structure in x-z plane at "j" = 6 (y = 5.50000E+03 meters).

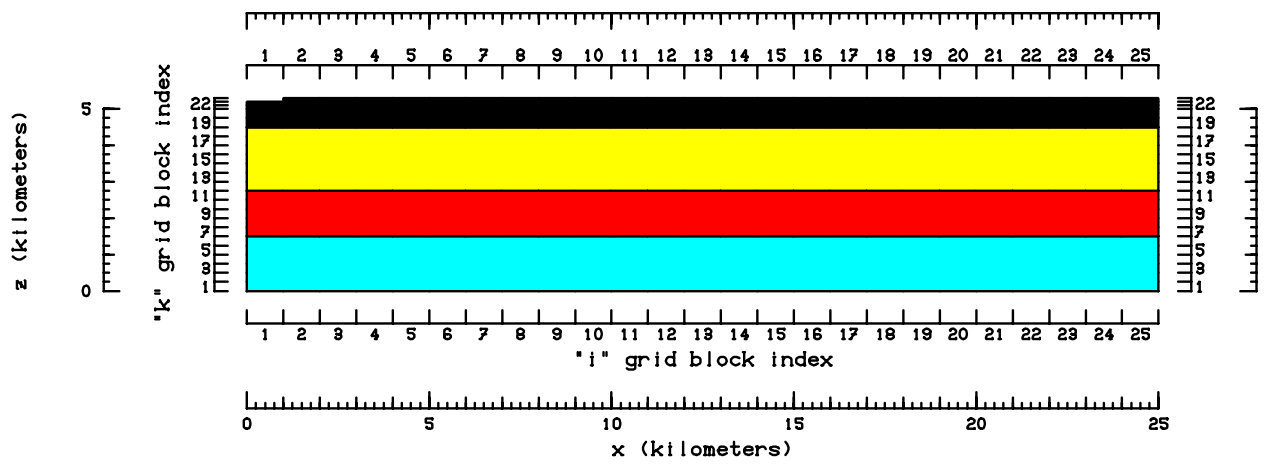


Figure 6g: Earth structure in x-z plane (j=6).

Underground earth structure in x-z plane at "j" = 7 (y = 6.5000E+03 meters).

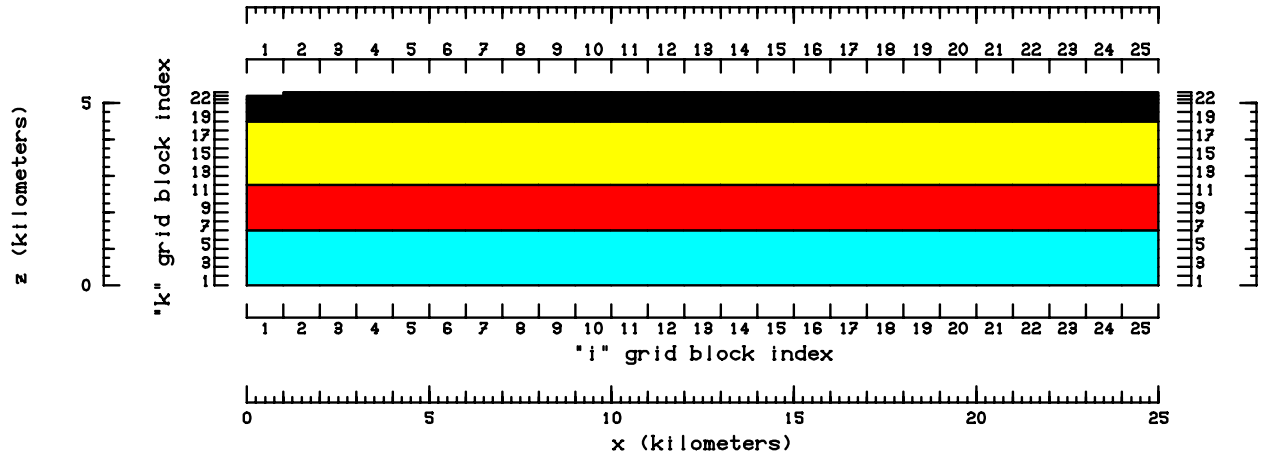


Figure 6h: Earth structure in x-z plane (j=7).

Underground earth structure in x-z plane at "j" = 8 (y = 7.5000E+03 meters).

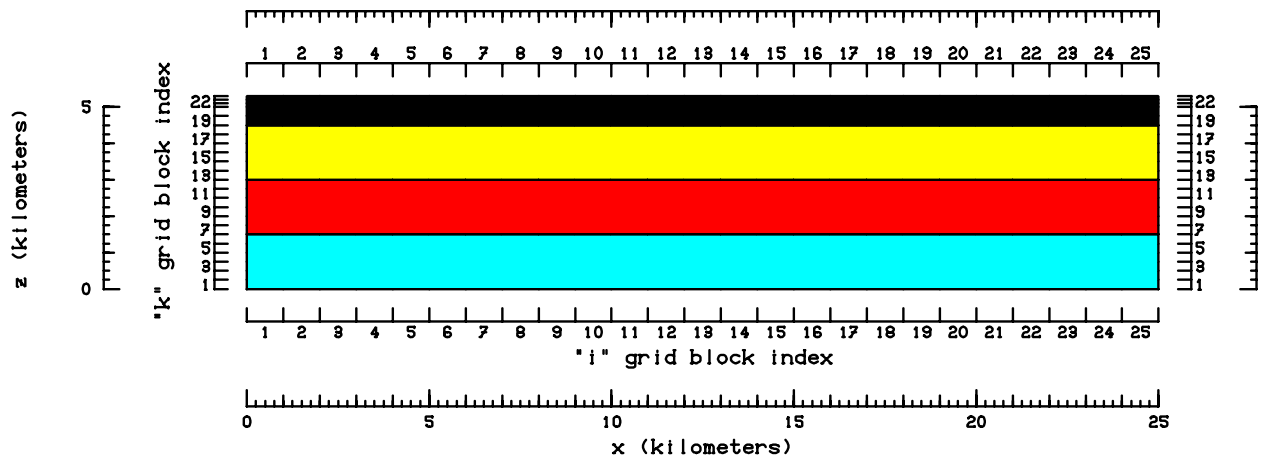


Figure 6i: Earth structure in x-z plane (j=8).

Underground earth structure in x-z plane at "j" = 9 (y = 8.50000E+03 meters).

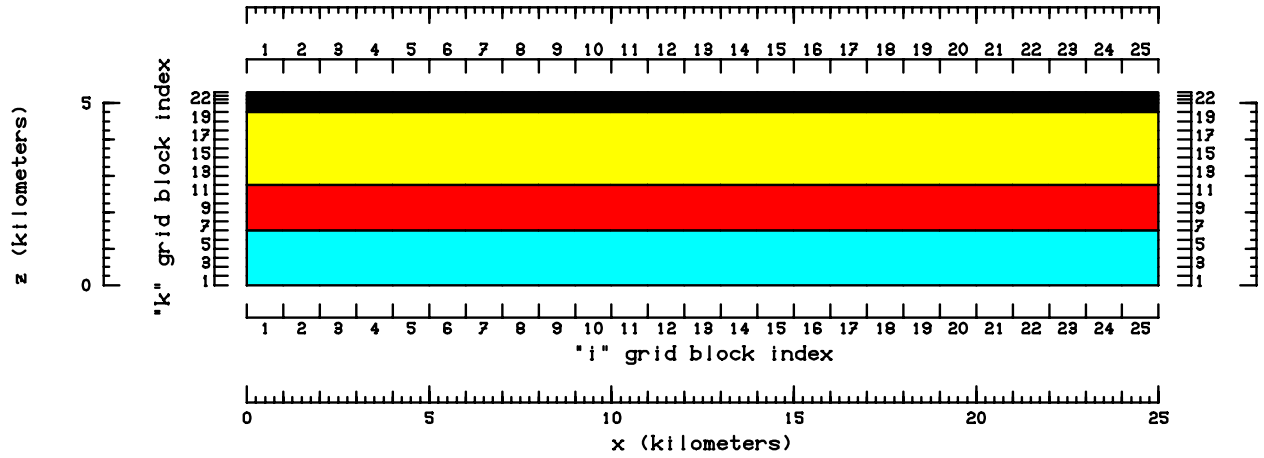


Figure 6j: Earth structure in x-z plane (j=9).

Underground earth structure in x-z plane at "j" = 10 (y = 9.50000E+03 meters).

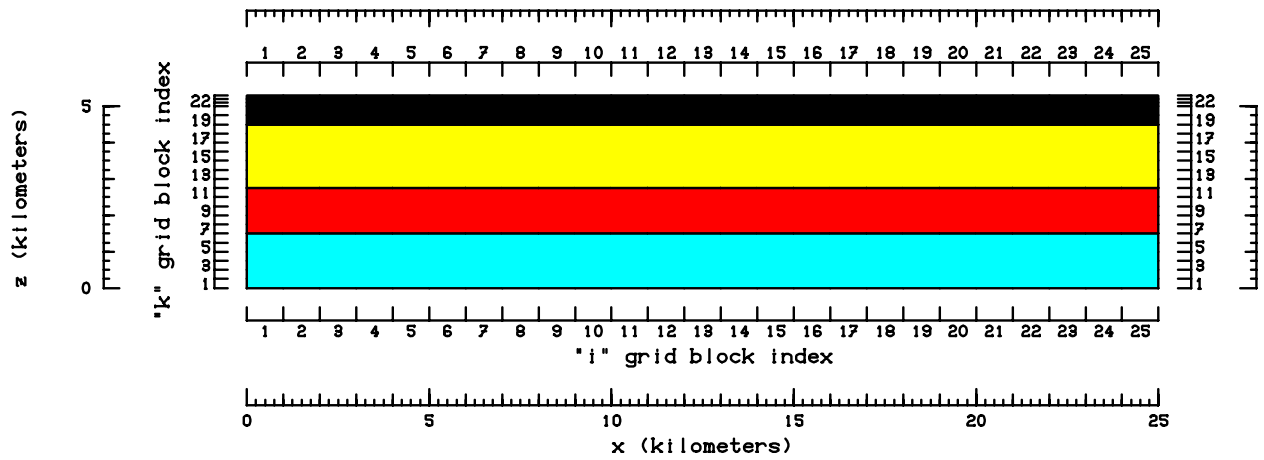


Figure 6k: Earth structure in x-z plane (j=10).

Underground earth structure in x-z plane at "j" = 11 (y = 1.05000E+04 meters).

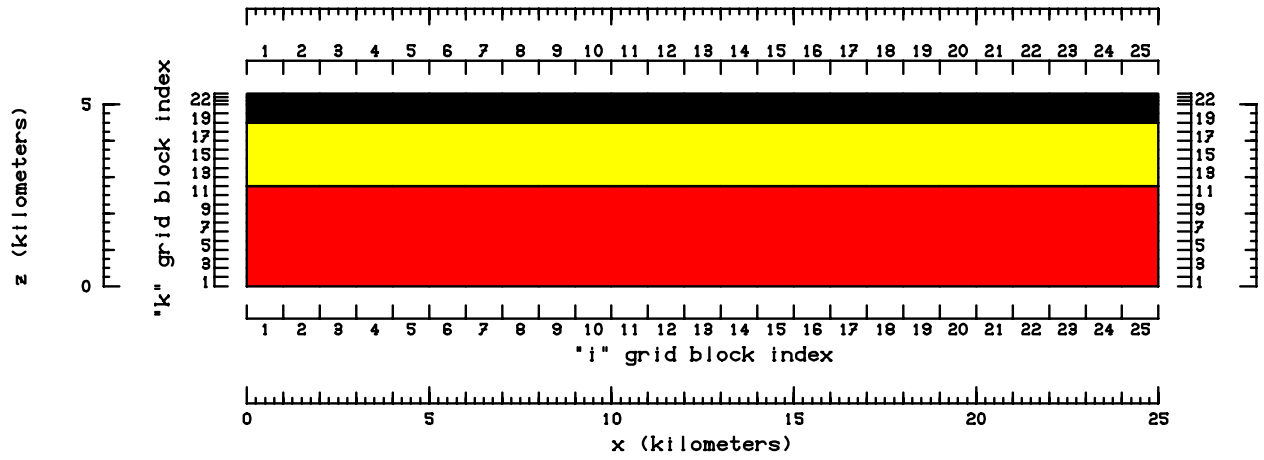


Figure 6l: Earth structure in x-z plane (j=11).

Underground earth structure in x-z plane at "j" = 12 (y = 1.15000E+04 meters).

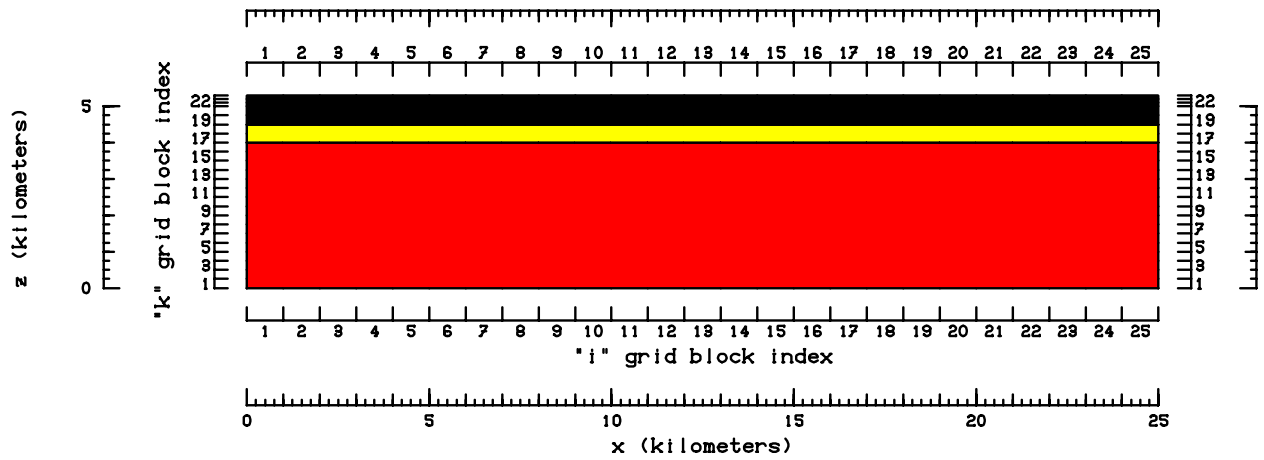


Figure 6m: Earth structure in x-z plane (j=12).

Underground earth structure in x-z plane at "j" = 13 (y = 1.25000E+04 meters).

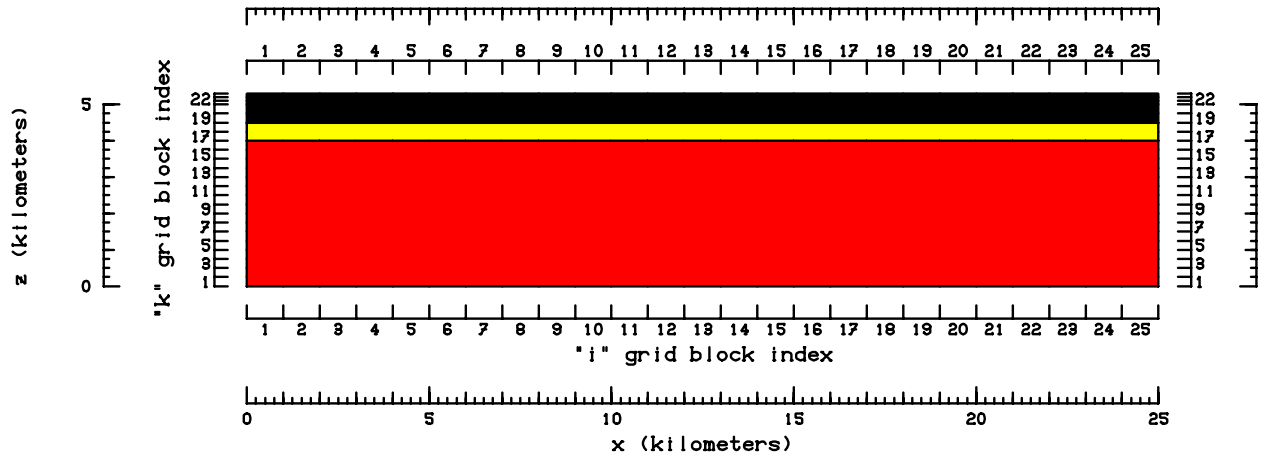


Figure 6n: Earth structure in x-z plane (j=13).

Underground earth structure in x-z plane at "j" = 14 (y = 1.35000E+04 meters).

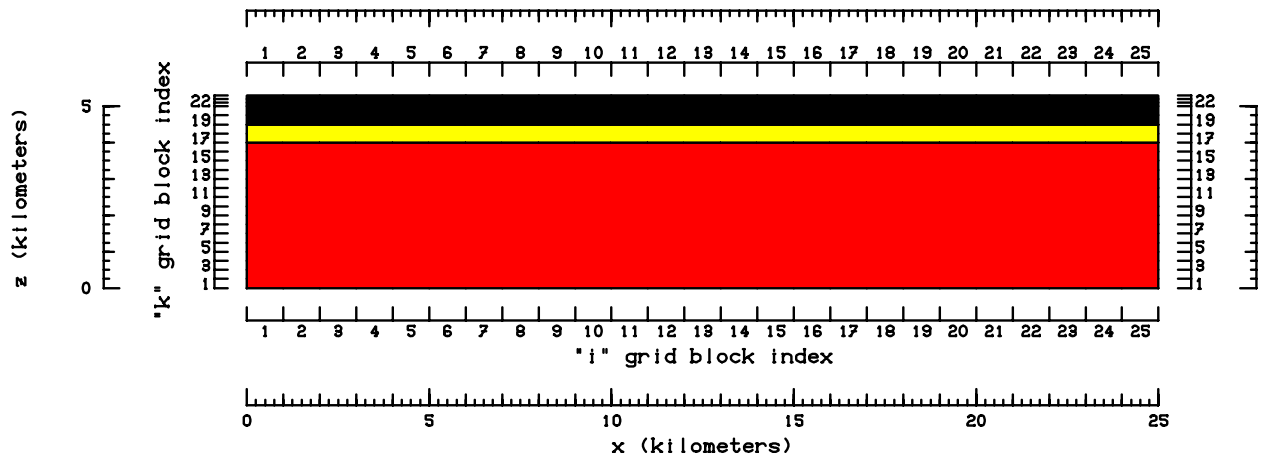


Figure 6o: Earth structure in x-z plane (j=14).

Underground earth structure in x-z plane at "j" = 15 (y = 1.45000E+04 meters).

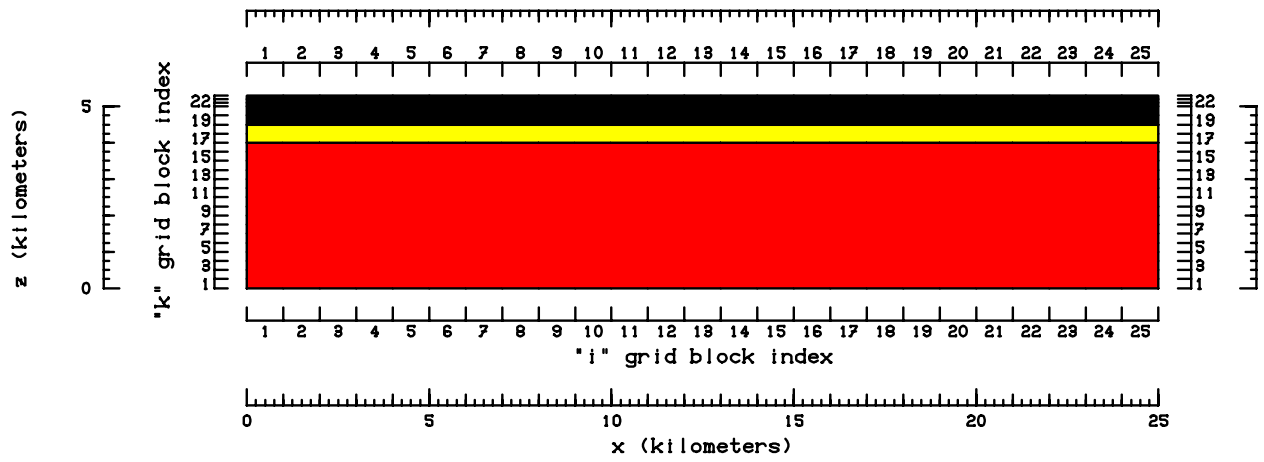


Figure 6p: Earth structure in x-z plane (j=15).

Underground earth structure in x-z plane at "j" = 16 (y = 1.55000E+04 meters).

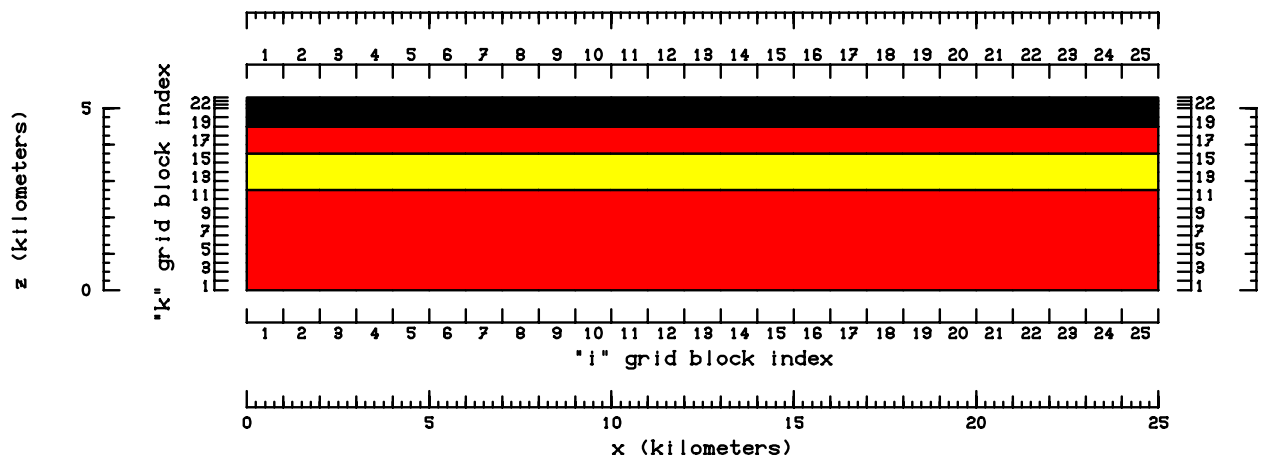


Figure 6q: Earth structure in x-z plane (j=16).

Underground earth structure in x-z plane at "j" = 17 (y = 1.65000E+04 meters).

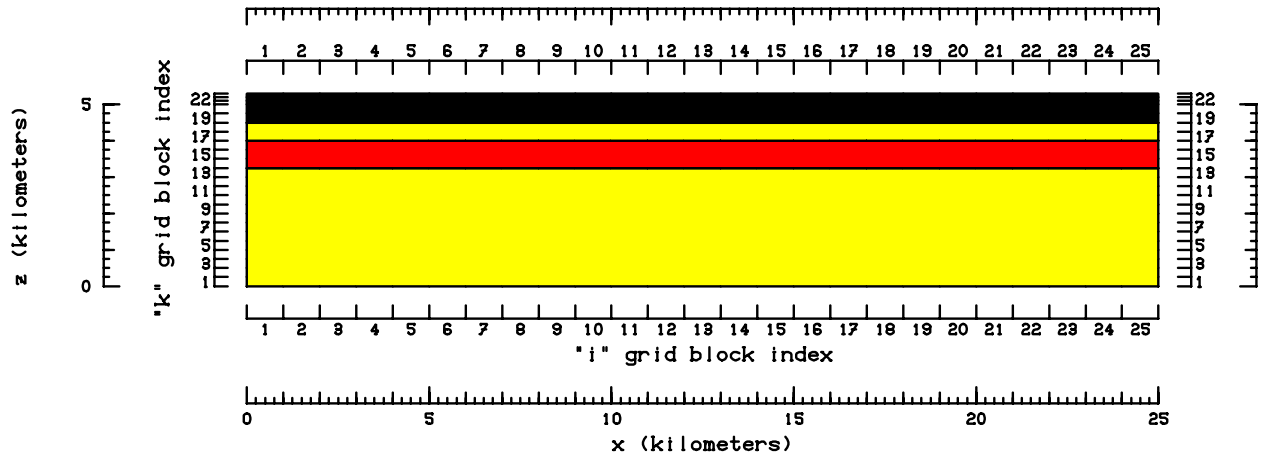


Figure 6r: Earth structure in x-z plane (j=17).

Underground earth structure in x-z plane at "j" = 18 (y = 1.75000E+04 meters).

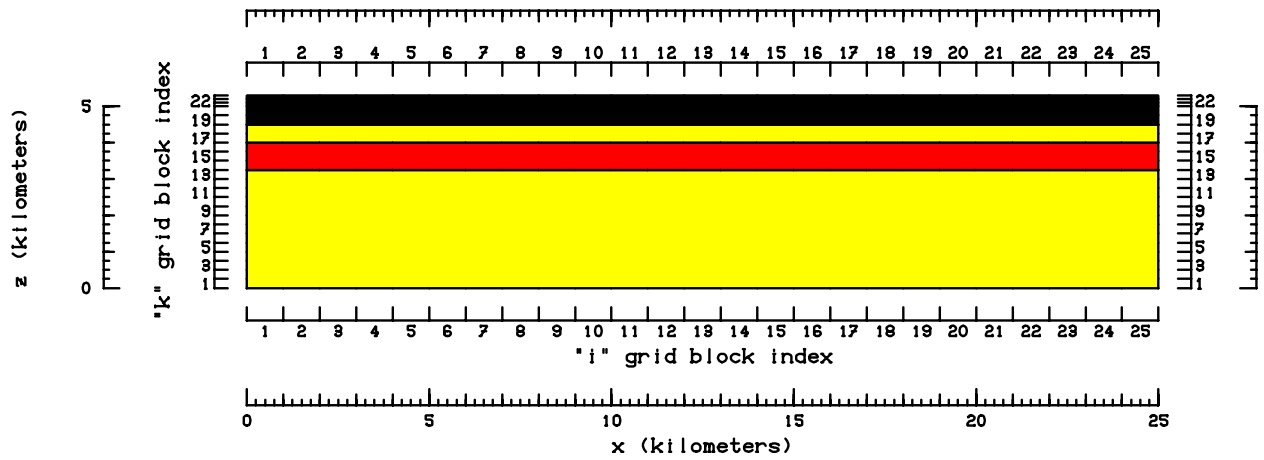


Figure 6s: Earth structure in x-z plane (j=18).

Underground earth structure in x-z plane at "j" = 19 (y = 1.85000E+04 meters).

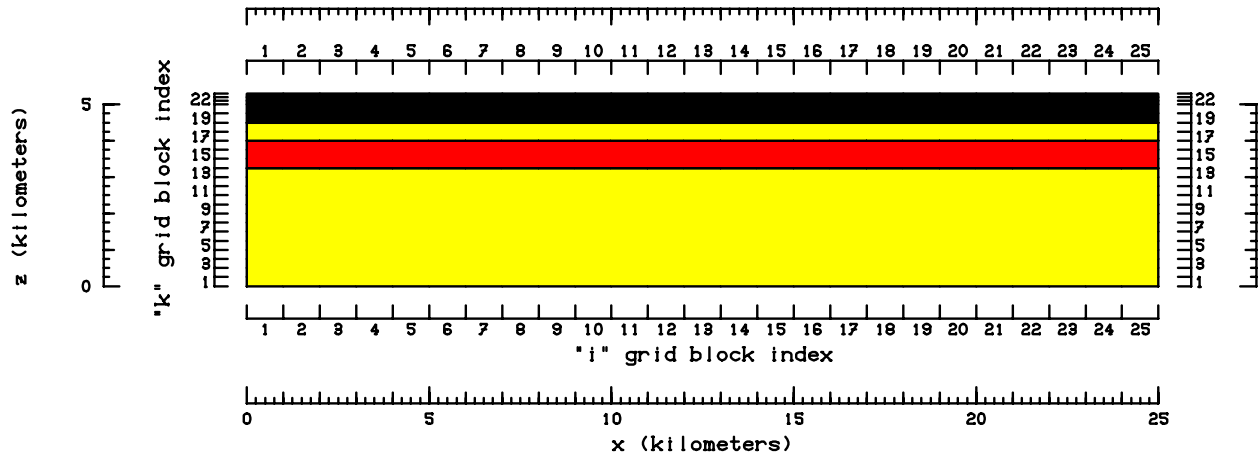


Figure 6t: Earth structure in x-z plane (j=19).

Underground earth structure in x-z plane at "j" = 20 (y = 1.95000E+04 meters).

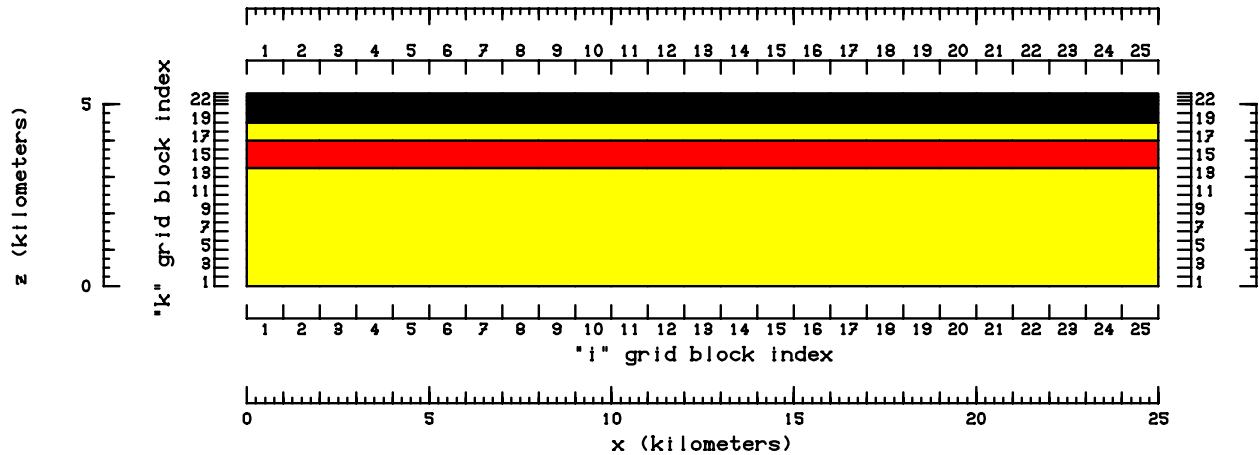


Figure 6u: Earth structure in x-z plane (j=20).

Along the top boundary, the water table (i.e. 1 bar surface) is assumed to be at an elevation given by:

$$z_w = 0.10(z - 720) + 720 = 0.10z + 648 \quad (1)$$

where  $z_w$  denotes the water table elevation (mASL) and  $z$  is the local ground surface elevation.

The ground surface temperature and shallow subsurface temperature gradient are assumed to be 10 °C and 80 °C/km, respectively. If the water table given by Eq. (1) falls below the mid-point of a grid block, the grid block is flagged as void. Use of Eq. (1) renders all of the grid blocks in layers  $k=24$  and  $k=25$ , and some grid blocks in layer  $k=23$  void. Sources and sinks are imposed in all the top-most grid blocks in each vertical column ( $i, j; i=1, \dots, 25$ , and  $j=1, \dots, 20$ ) to maintain the pressures and temperatures consistent with Eq. (1), and the assumed surface temperature and shallow subsurface temperature gradient.

Along the bottom boundary, a uniform conductive heat flux ( $120 \text{ mW/m}^2$ ) is imposed along the entire surface. All the vertical faces of the grid are assumed to be impermeable and insulated. The reservoir fluid is treated as pure water.

### **III. Computation of Quasi-Steady Natural State**

Starting from an essentially arbitrary cold state, the computation was marched forward in time for about 625,000 years. The maximum time step used was 25 years. The change in total thermal energy and fluid mass in the computational grid is displayed in Figures 7 and 8. For most of the computational period, the thermal energy continues to increase and the fluid mass declines. Initially the change is rapid; it moderates over time. After about 500,000, the change is quite small over a time scale of 50 to 100 years. The computed temperature values at cycle 25,000 (about 625,000 years) were compared with the available data.

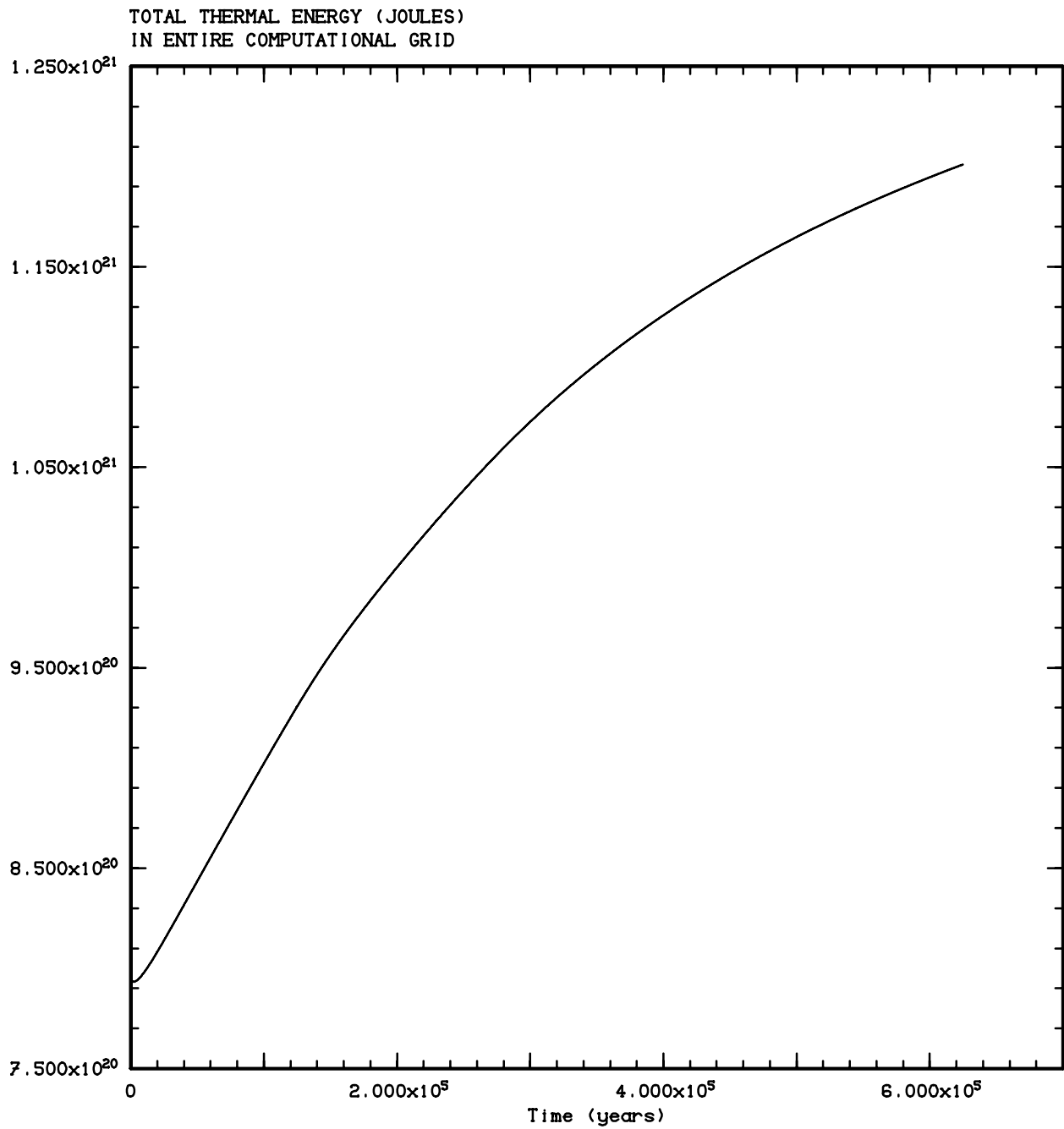


Figure 7: Computed total thermal energy in the computational grid.

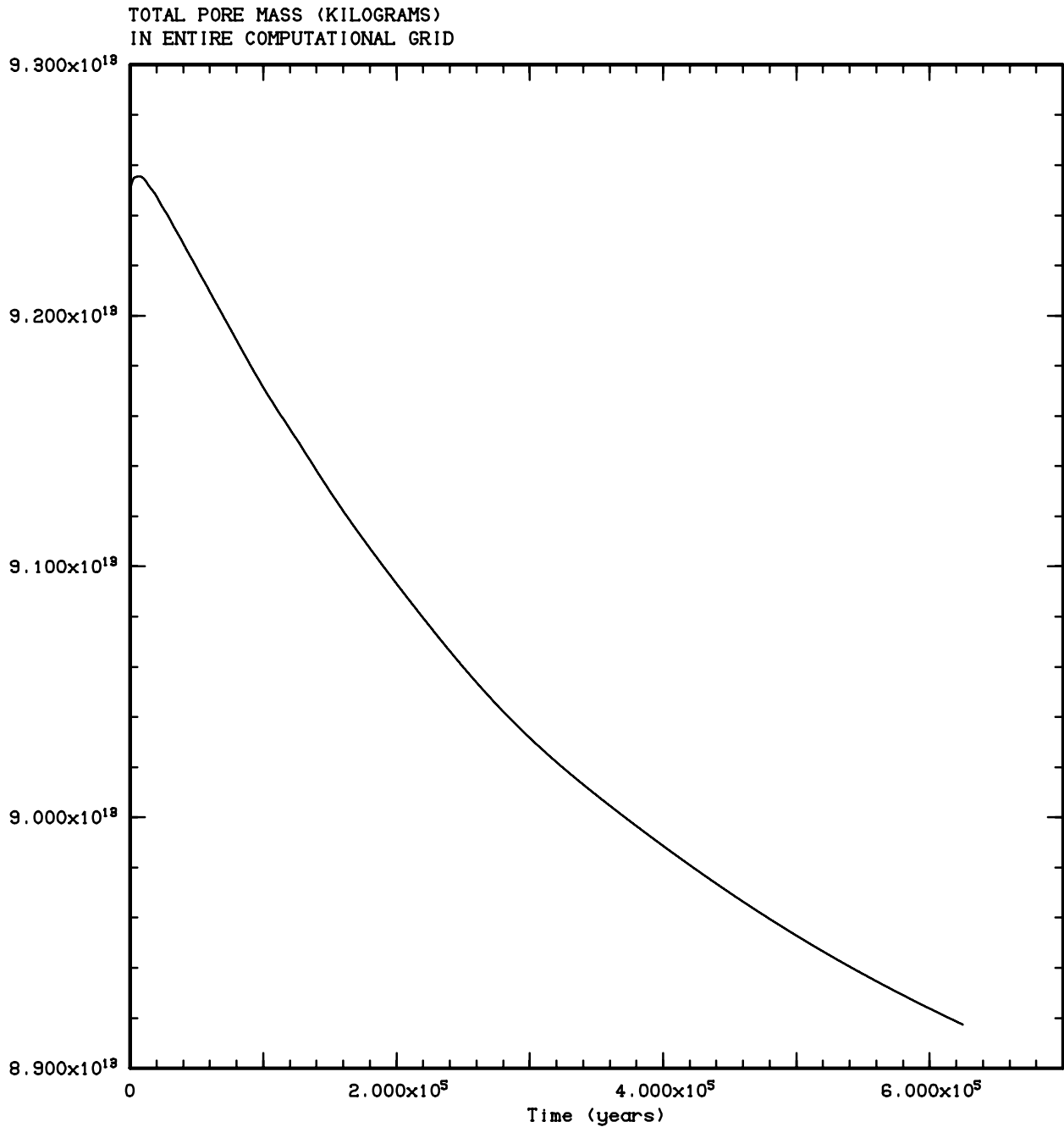


Figure 8: Computed total fluid mass in the computational grid.

The measured temperatures in Mountain Home wells MH-1 and MH-2 are compared with calculated results from the model in Figures 9a-b. It is not known if the available temperature data represent stable formation temperatures. No information on shut-in time is available regarding the temperature surveys. Given the current data limitations, the agreement between the measured and computed temperature values is considered satisfactory.

Computed Underground Temperature Profile Near Well MH-1

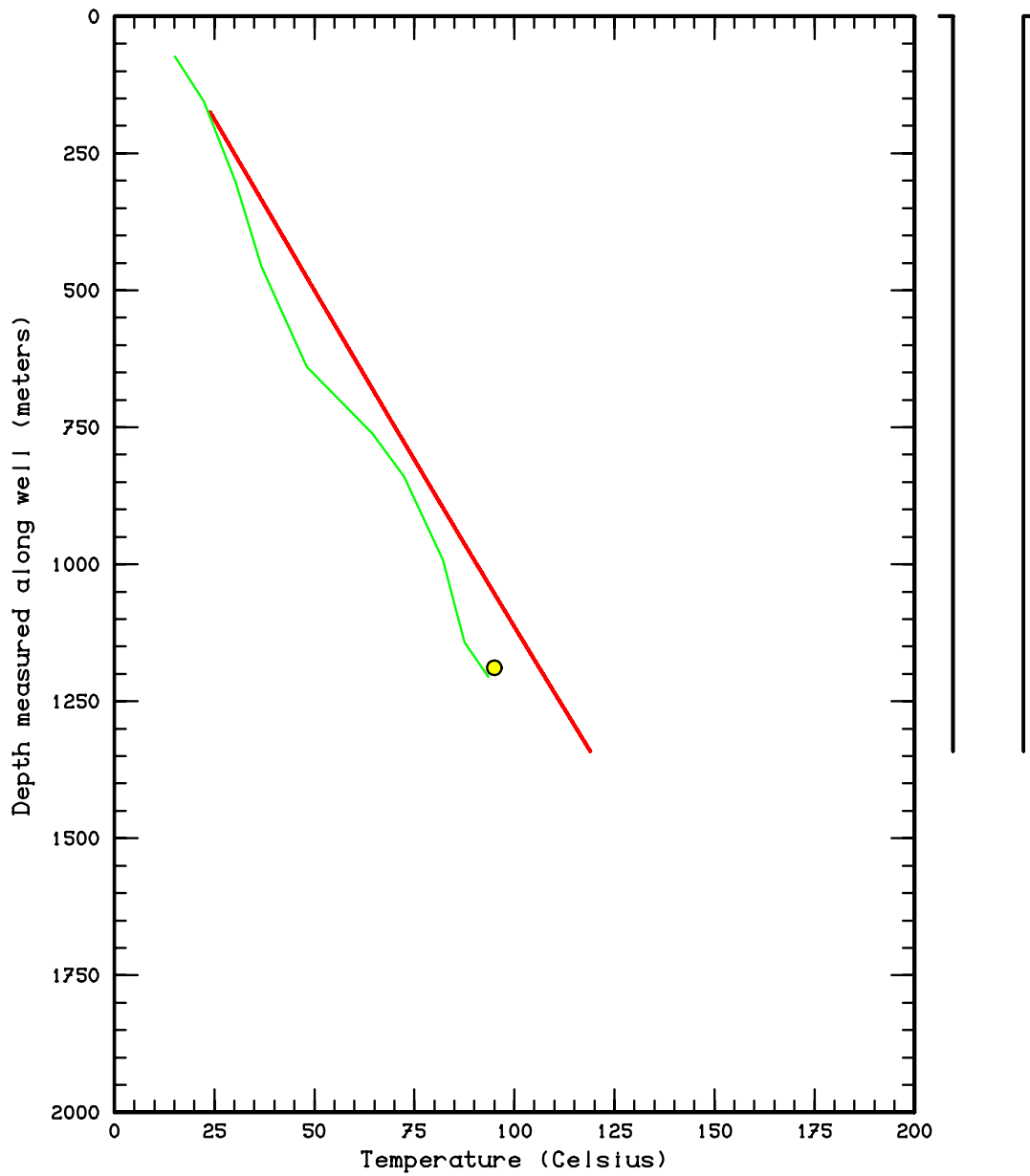


Figure 9a: Comparison between computed (solid red line) and measured temperature profiles (solid green line and yellow circle) for well MH-1. No information is available concerning the shut-in time at which the temperature survey was taken.

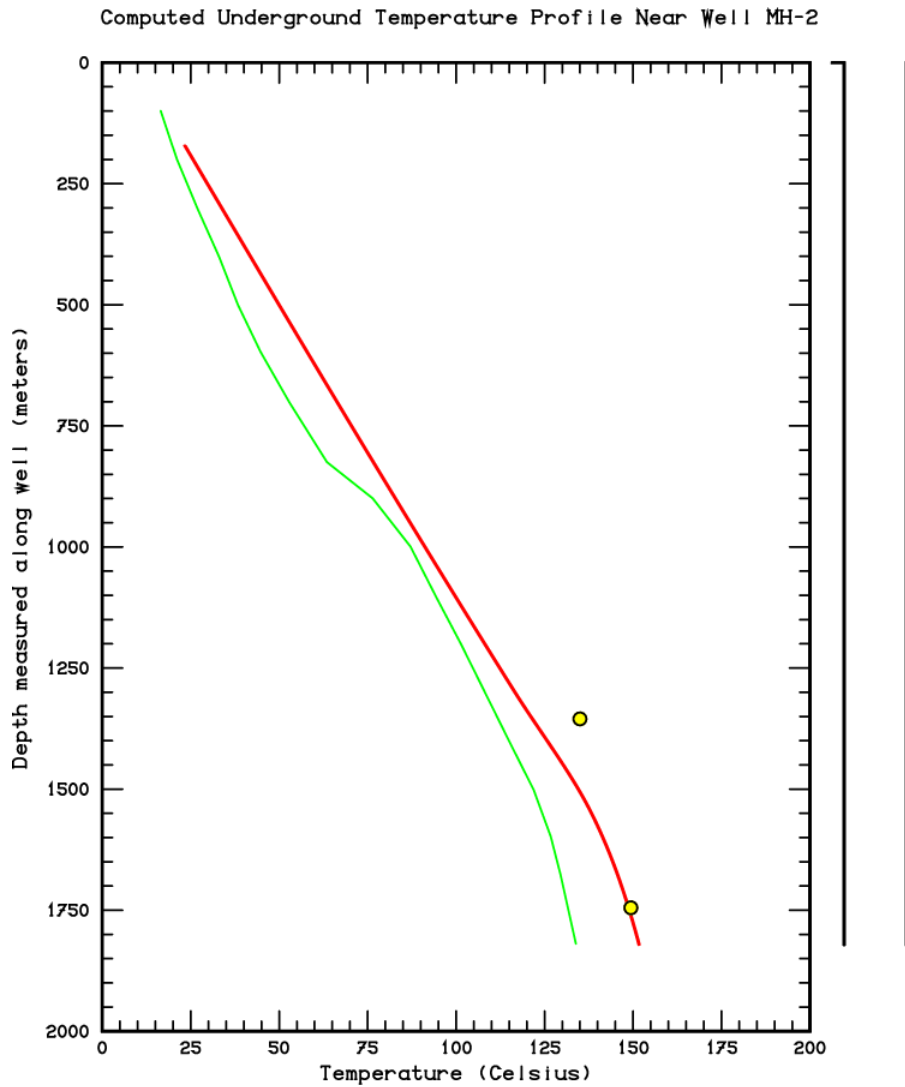


Figure 9b: Comparison between computed (solid red line) and measured temperature profiles (solid green line) for well MH-2. No information is available concerning the shut-in time at which the temperature survey was taken. The yellow circles are the measured flowing temperatures. Since the measured flowing temperatures are higher than the recorded shut-in temperatures (solid green line), it is almost certain that the shut-in survey does not represent the stable formation temperatures.

#### IV. Computed Temperature Distribution and Fluid Flow

Computed temperatures and fluid flux vectors in horizontal x-y ( $k=1$  to  $k=23$ ) and vertical x-z ( $j=1$  to  $j=20$ ) planes are exhibited in Figures 10 and 11, respectively. Figures 11a to 11d ( $j=1$  to 4) and 11q-11t ( $j=17$  to 20) show little or no convective flow. The convective flow is limited to the lower half (i.e. below about 2500 m depth) along  $j=5$  to  $j=11$  (Figures 11a to 11 k); it extends to relatively shallow depths (about 1000 to 1500 m) along  $j=12$  to 16. Significant fluid flow is restricted to permeable basalt layer (lower basalt layer in Figure 6). Isotherms in Figures 10 exhibit the existence of convective cells in the north-central, corresponding to  $j=12$  to 16, portion of the grid.

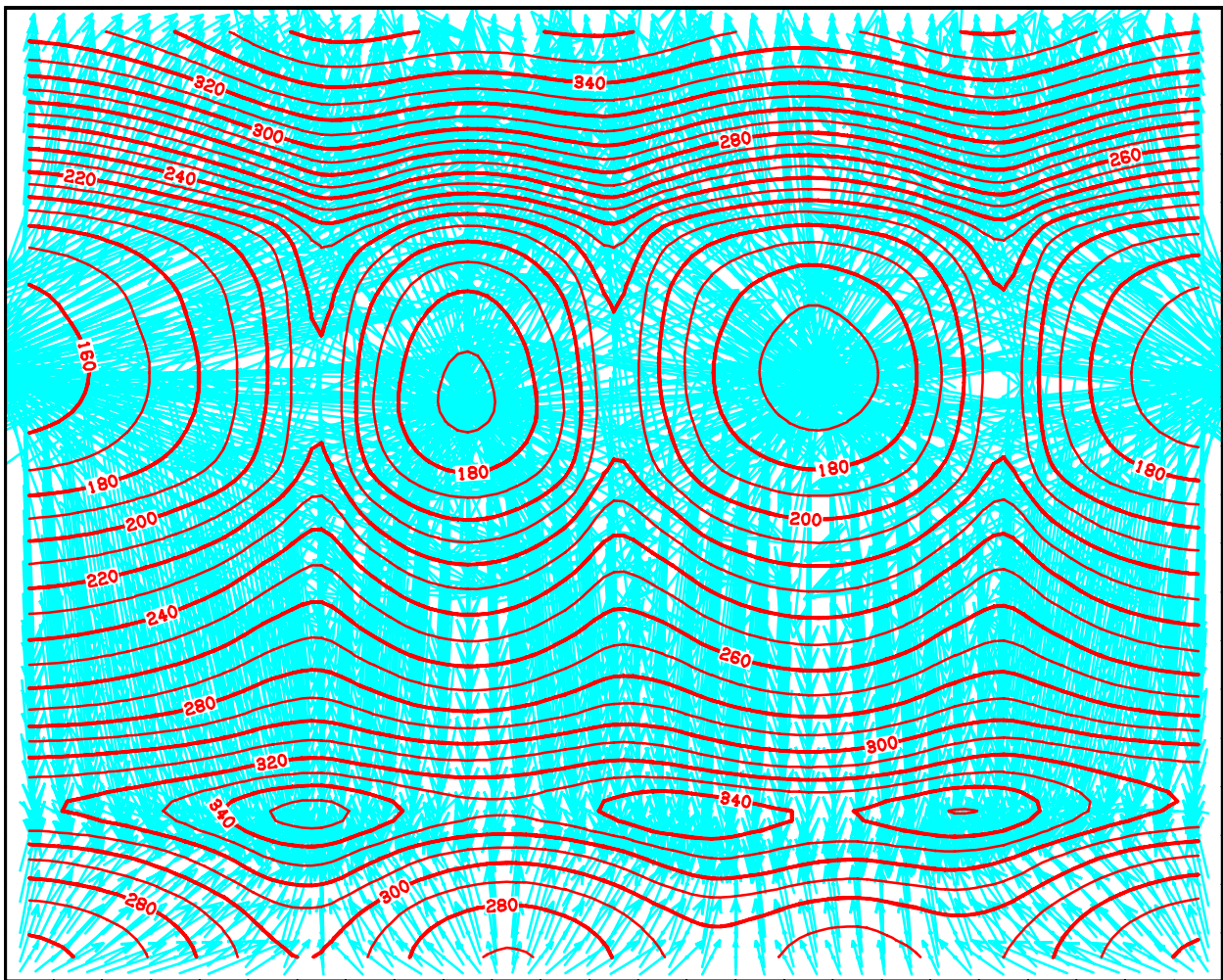


Figure 10a: Isotherms (red lines) and flow vectors (blue) in the horizontal x-y plane  $k=1$ .

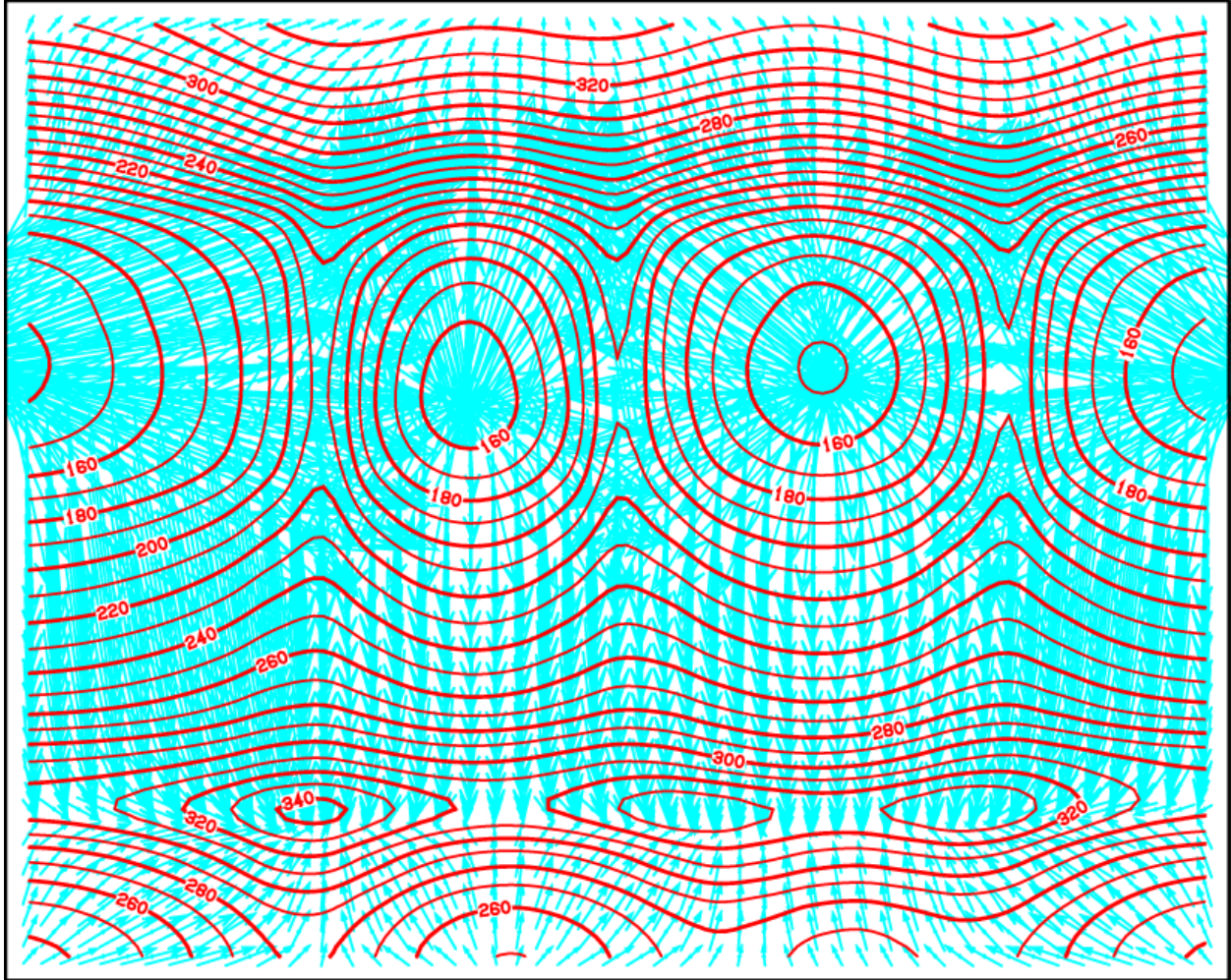


Figure 10b: Isotherms (red lines) and flow vectors (blue) in the horizontal x-y plane  $k=2$ .

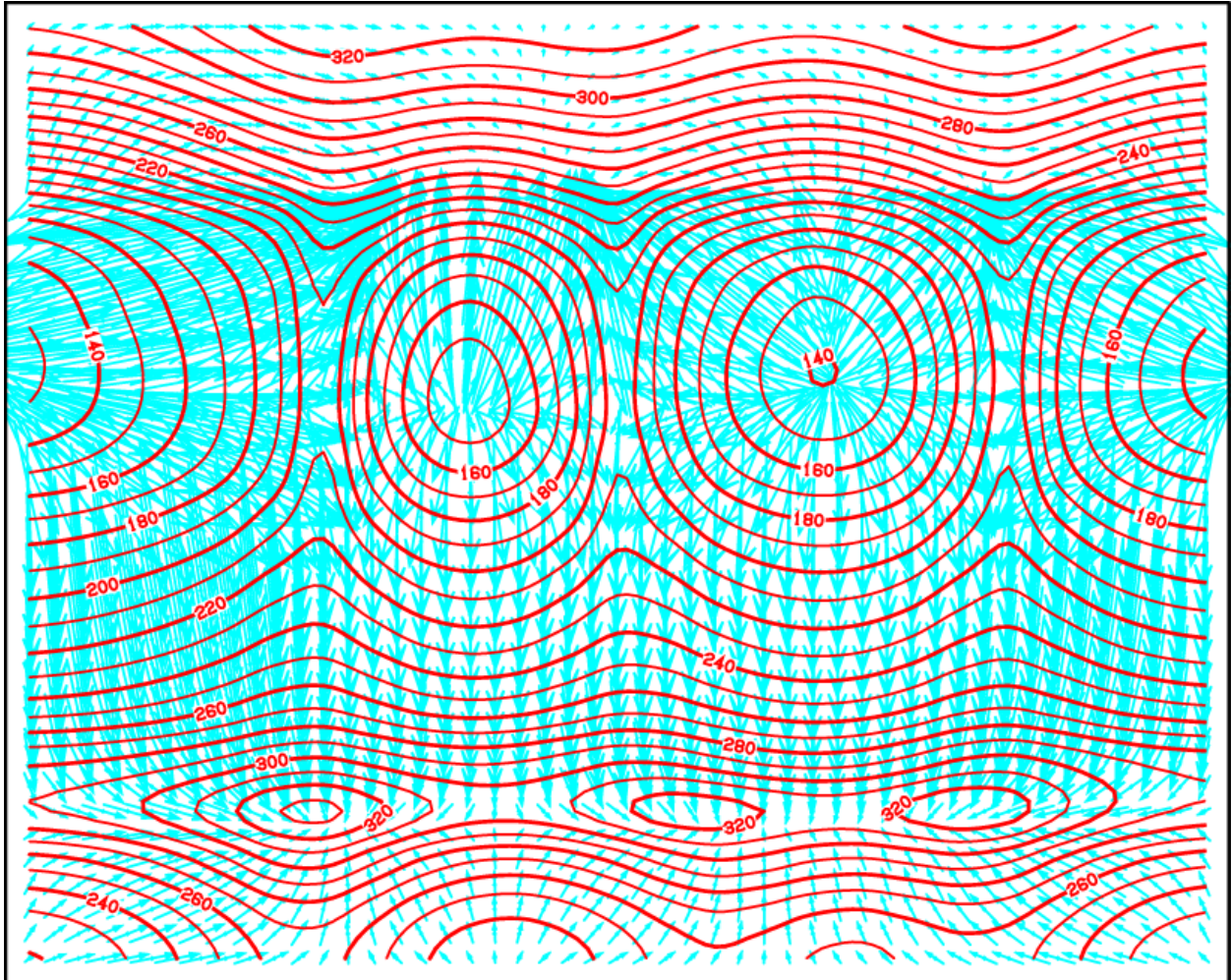


Figure 10c: Isotherms (red lines) and flow vectors (blue) in the horizontal x-y plane  $k=3$ .

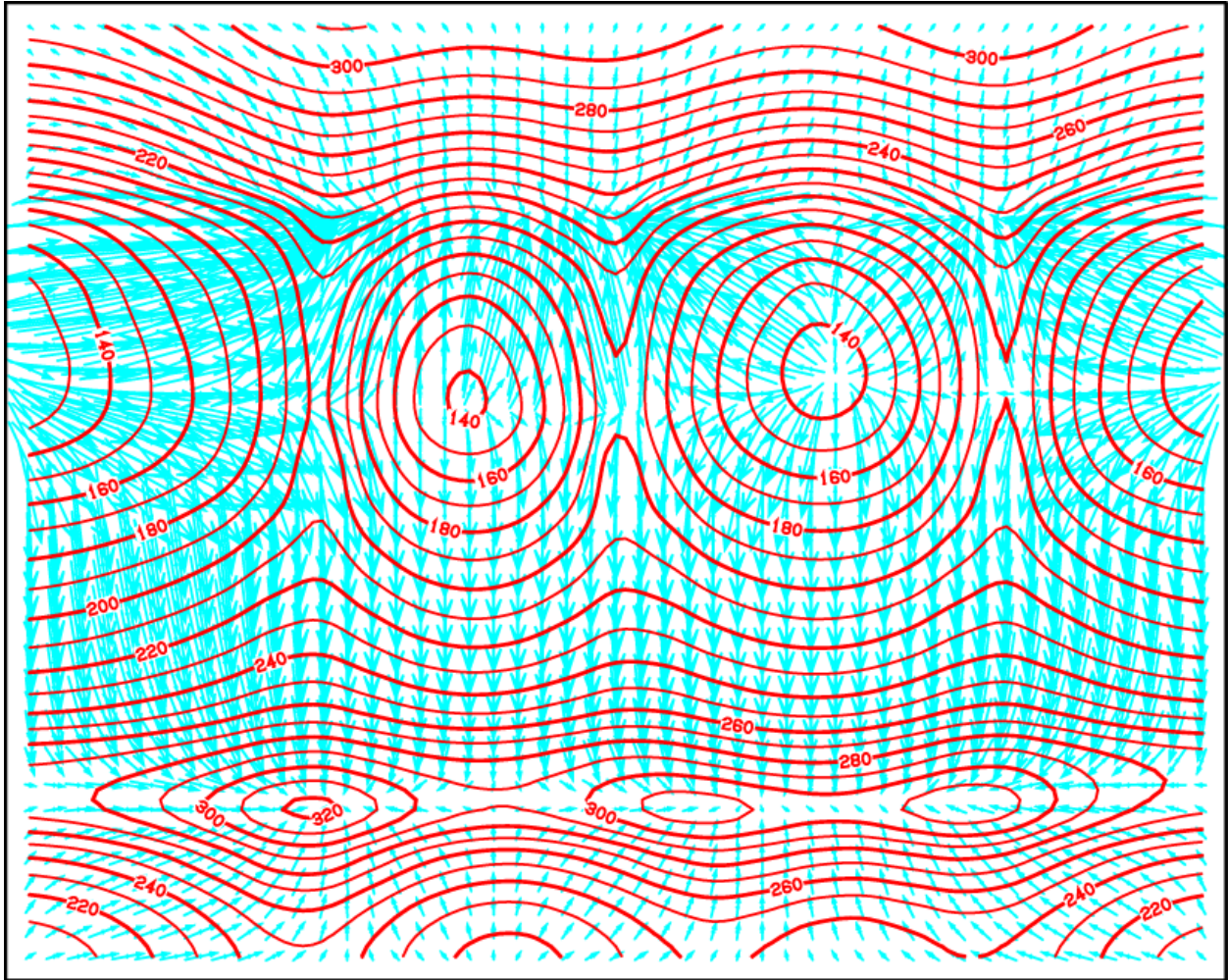


Figure 10d: Isotherms (red lines) and flow vectors (blue) in the horizontal x-y plane  $k=4$ .

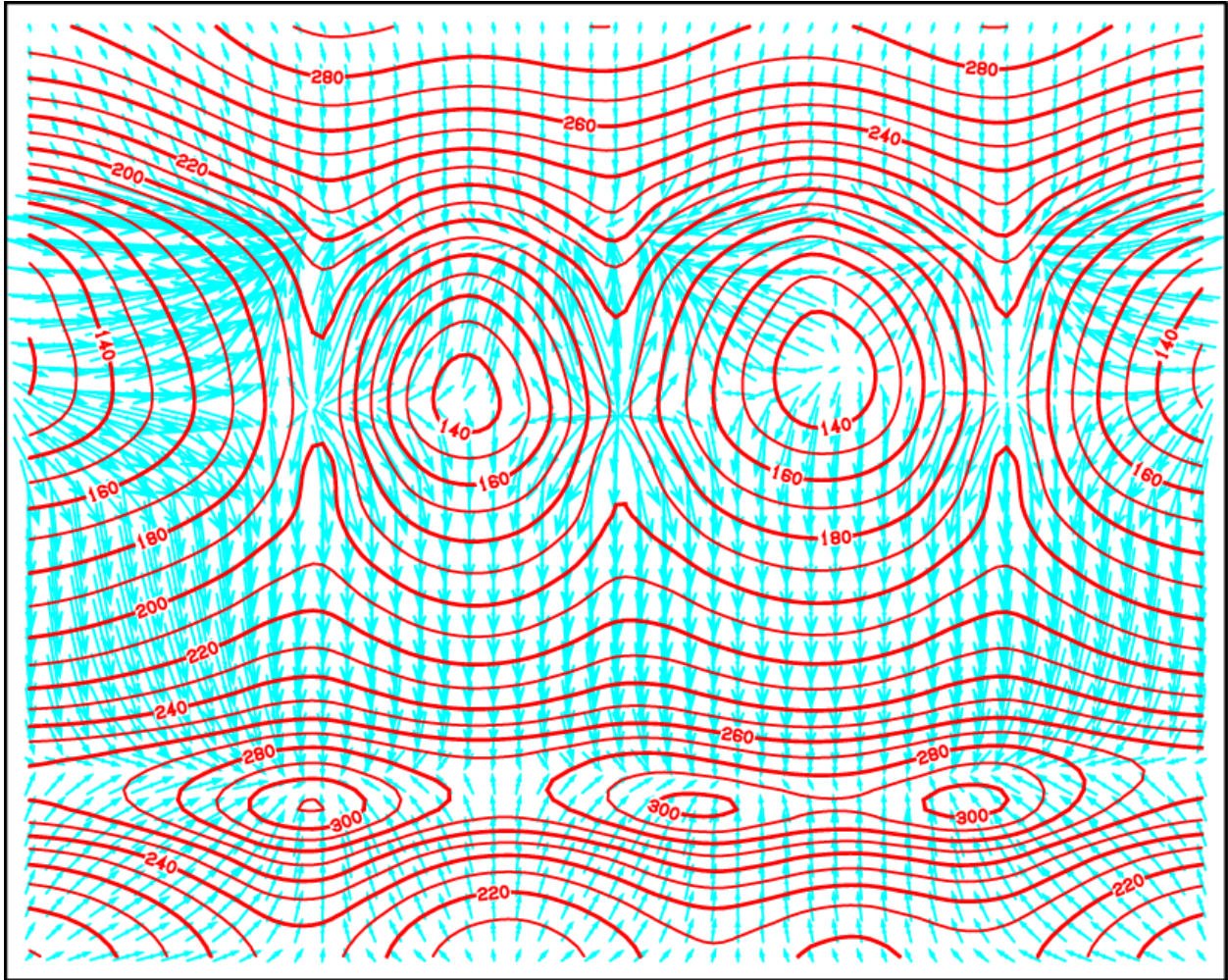


Figure 10e: Isotherms (red lines) and flow vectors (blue) in the horizontal x-y plane  $k=5$ .

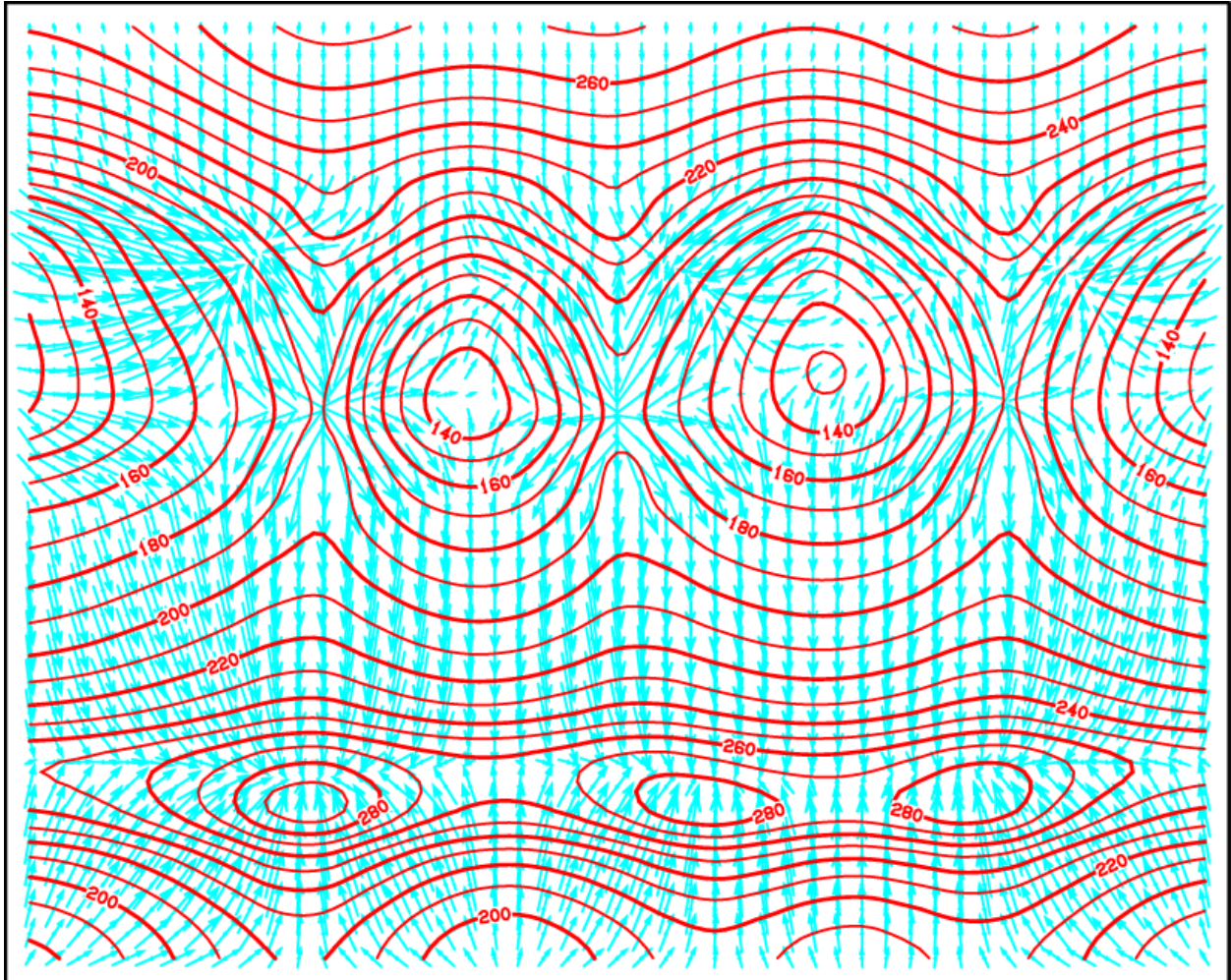


Figure 10f: Isotherms (red lines) and flow vectors (blue) in the horizontal x-y plane  $k=6$ .

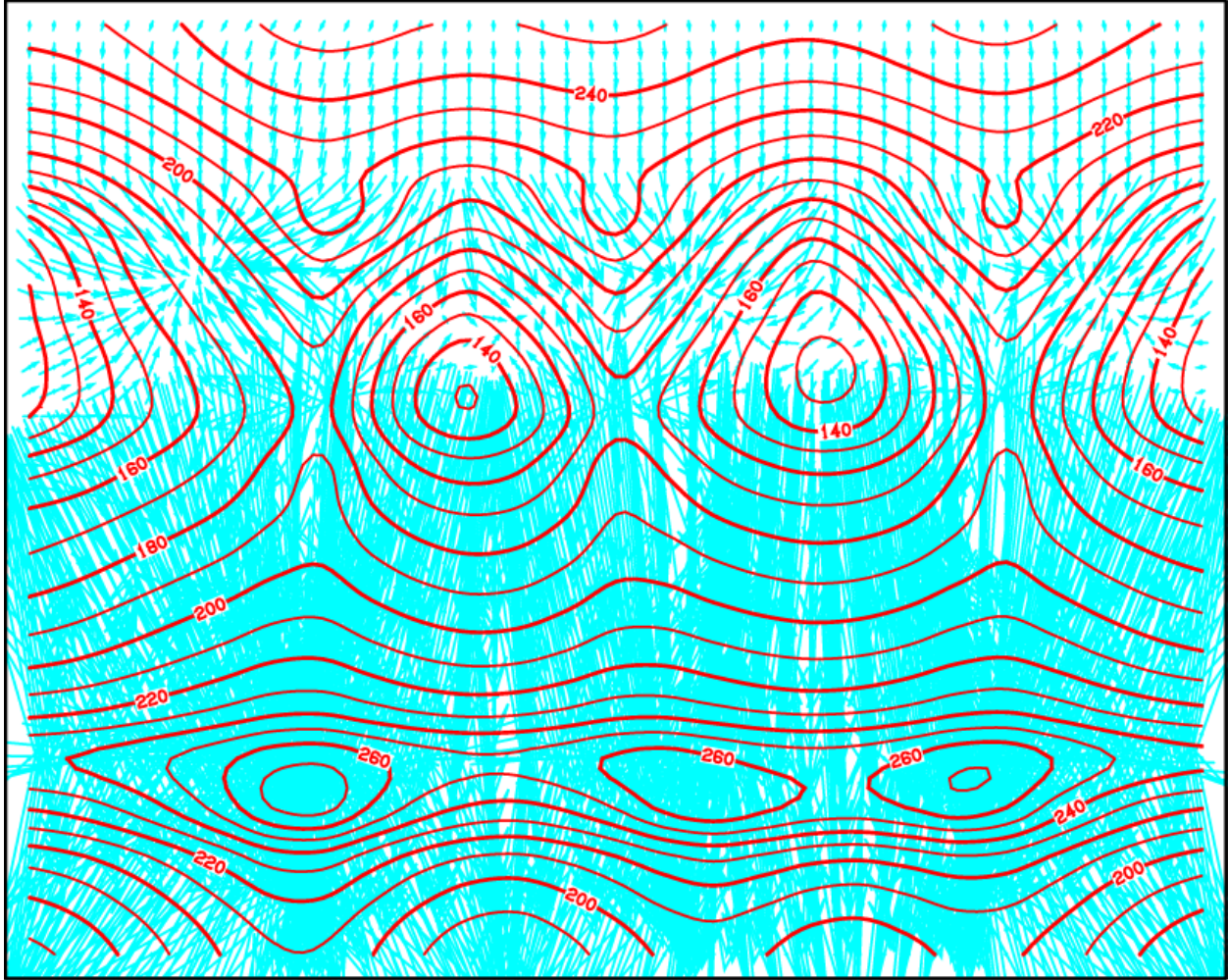


Figure 10g: Isotherms (red lines) and flow vectors (blue) in the horizontal x-y plane  $k=7$ .

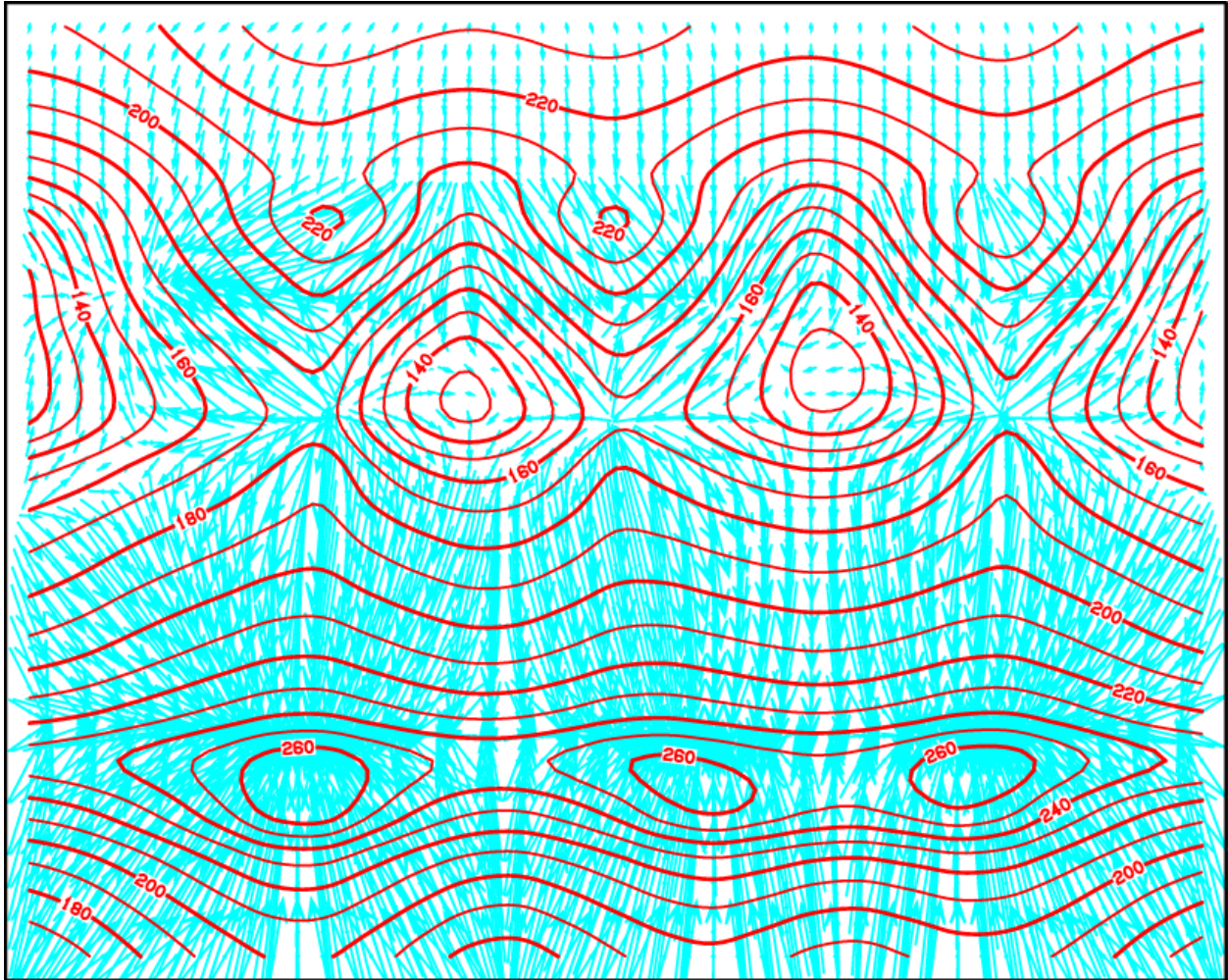


Figure 10h: Isotherms (red lines) and flow vectors (blue) in the horizontal x-y plane  $k=8$ .

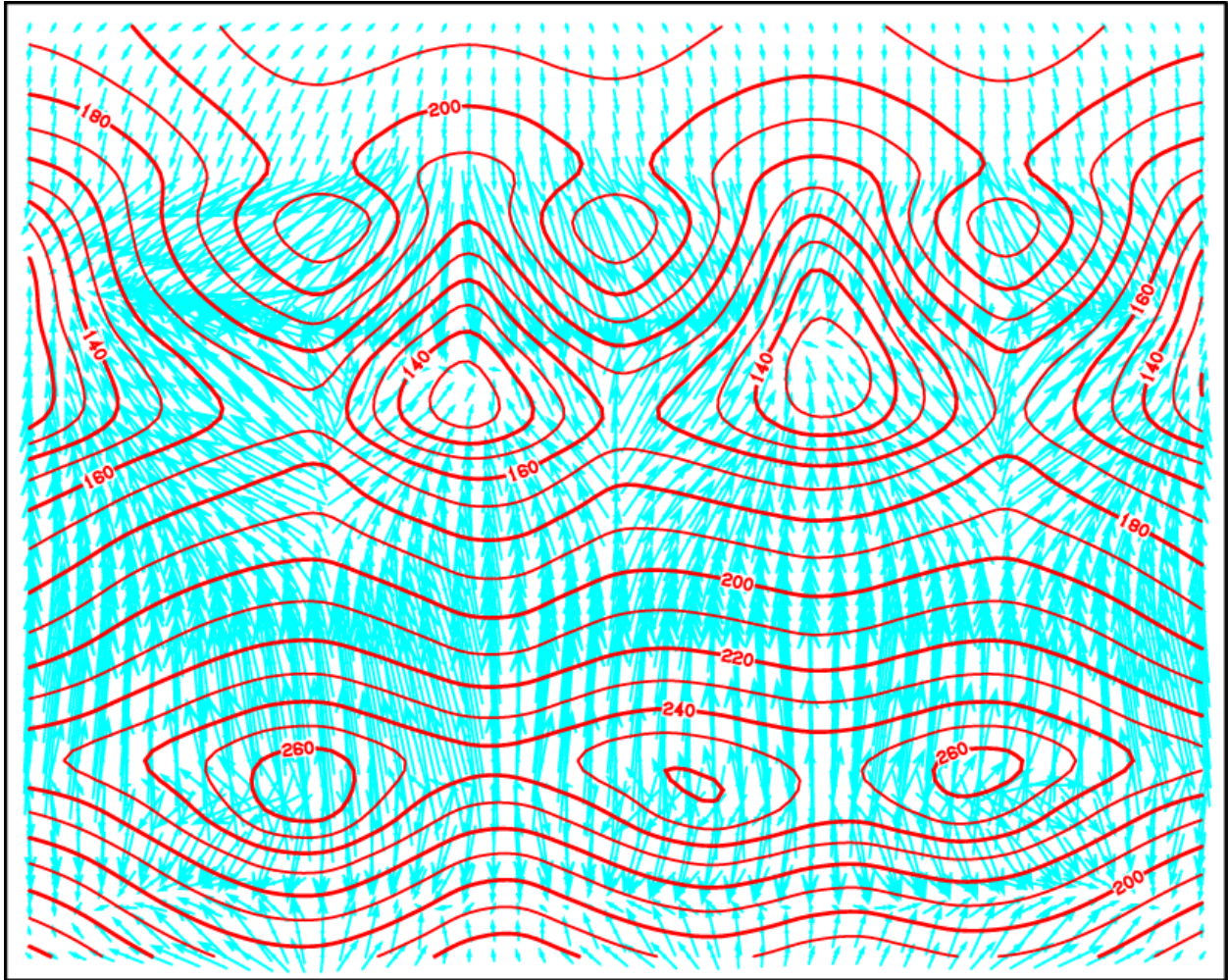


Figure 10i: Isotherms (red lines) and flow vectors (blue) in the horizontal x-y plane  $k=9$ .

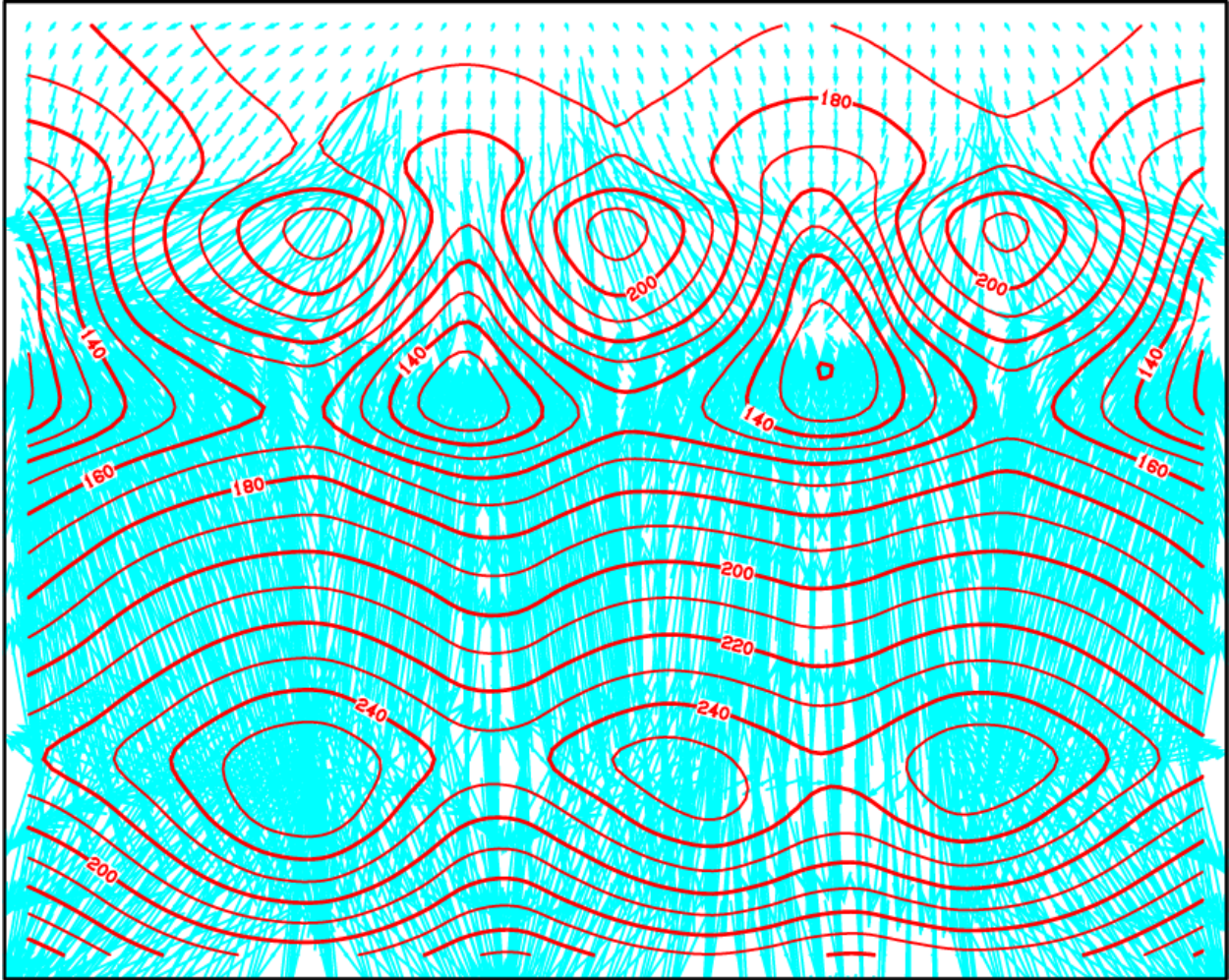


Figure 10j: Isotherms (red lines) and flow vectors (blue) in the horizontal x-y plane  $k=10$ .

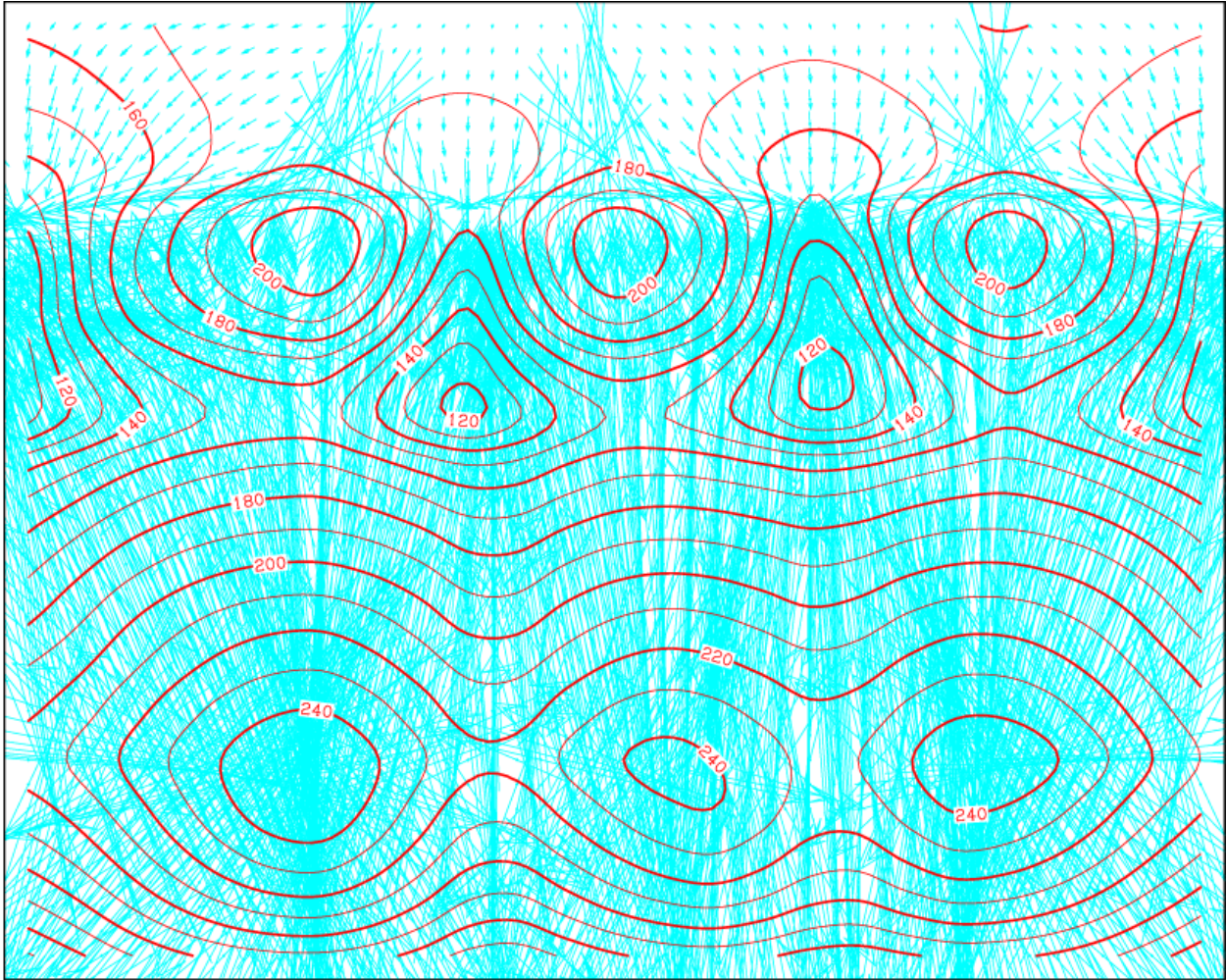


Figure 10k: Isotherms (red lines) and flow vectors (blue) in the horizontal x-y plane  $k=11$ .

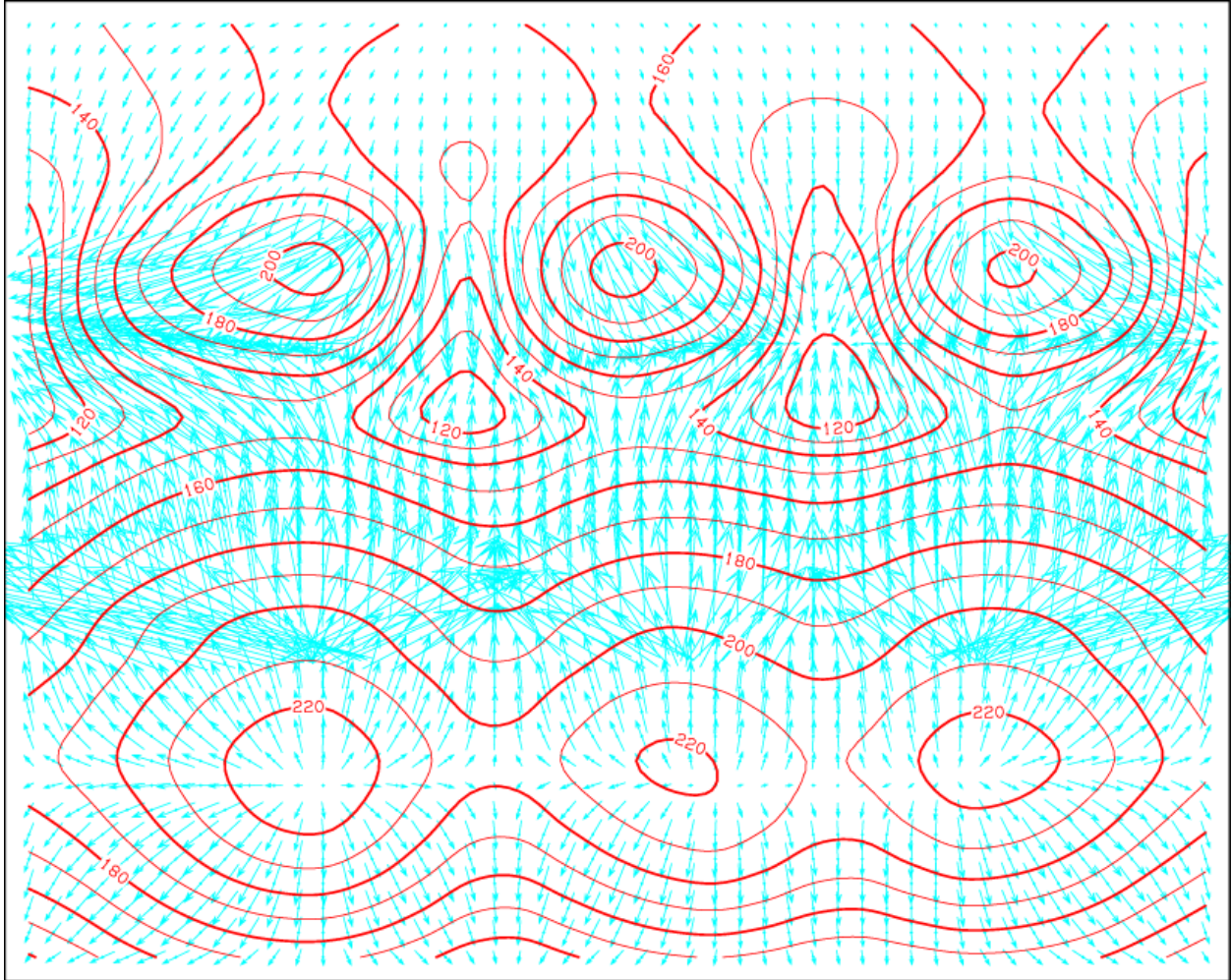


Figure 10l: Isotherms (red lines) and flow vectors (blue) in the horizontal x-y plane  $k=12$ .

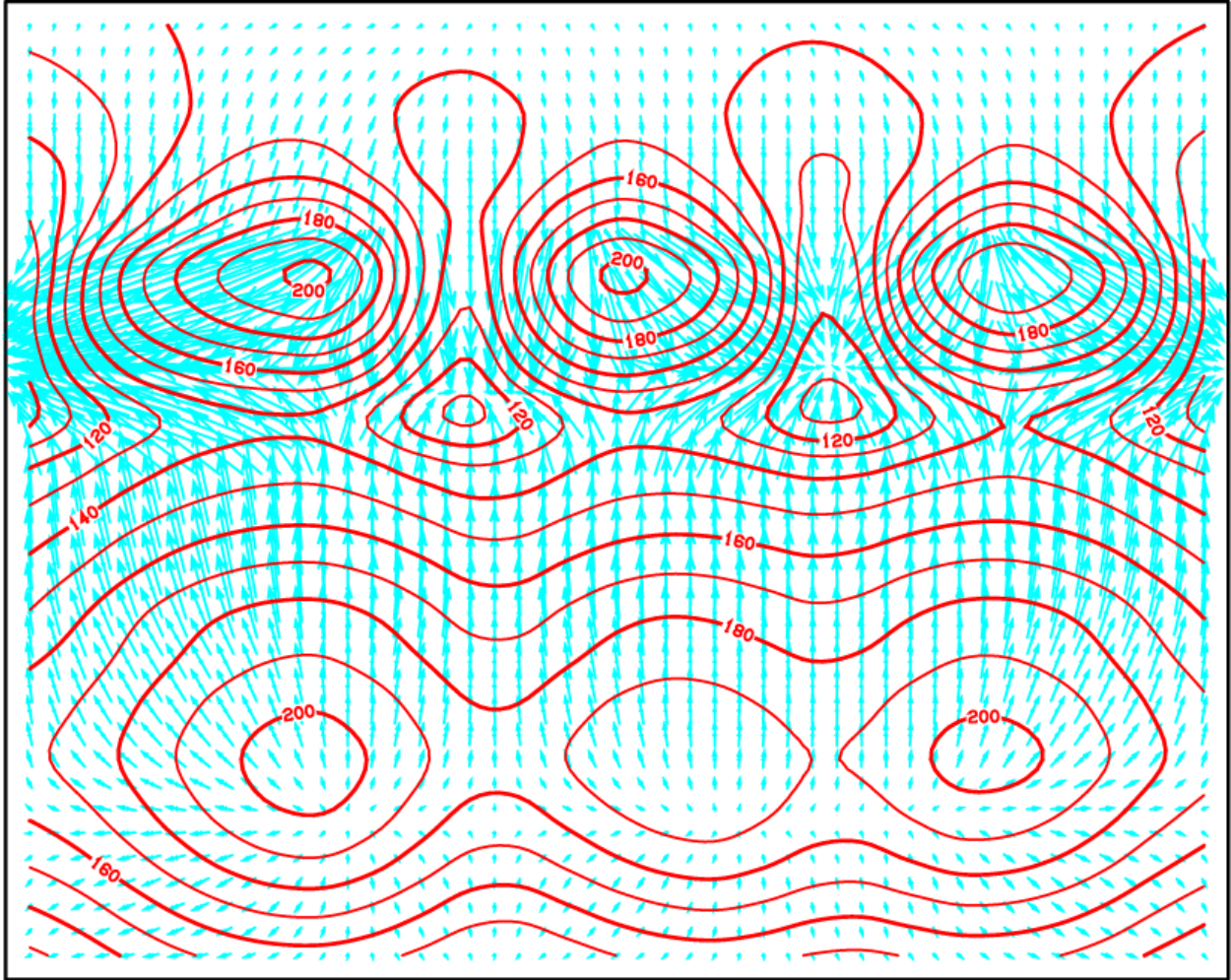


Figure 10m: Isotherms (red lines) and flow vectors (blue) in the horizontal x-y plane  $k=13$ .

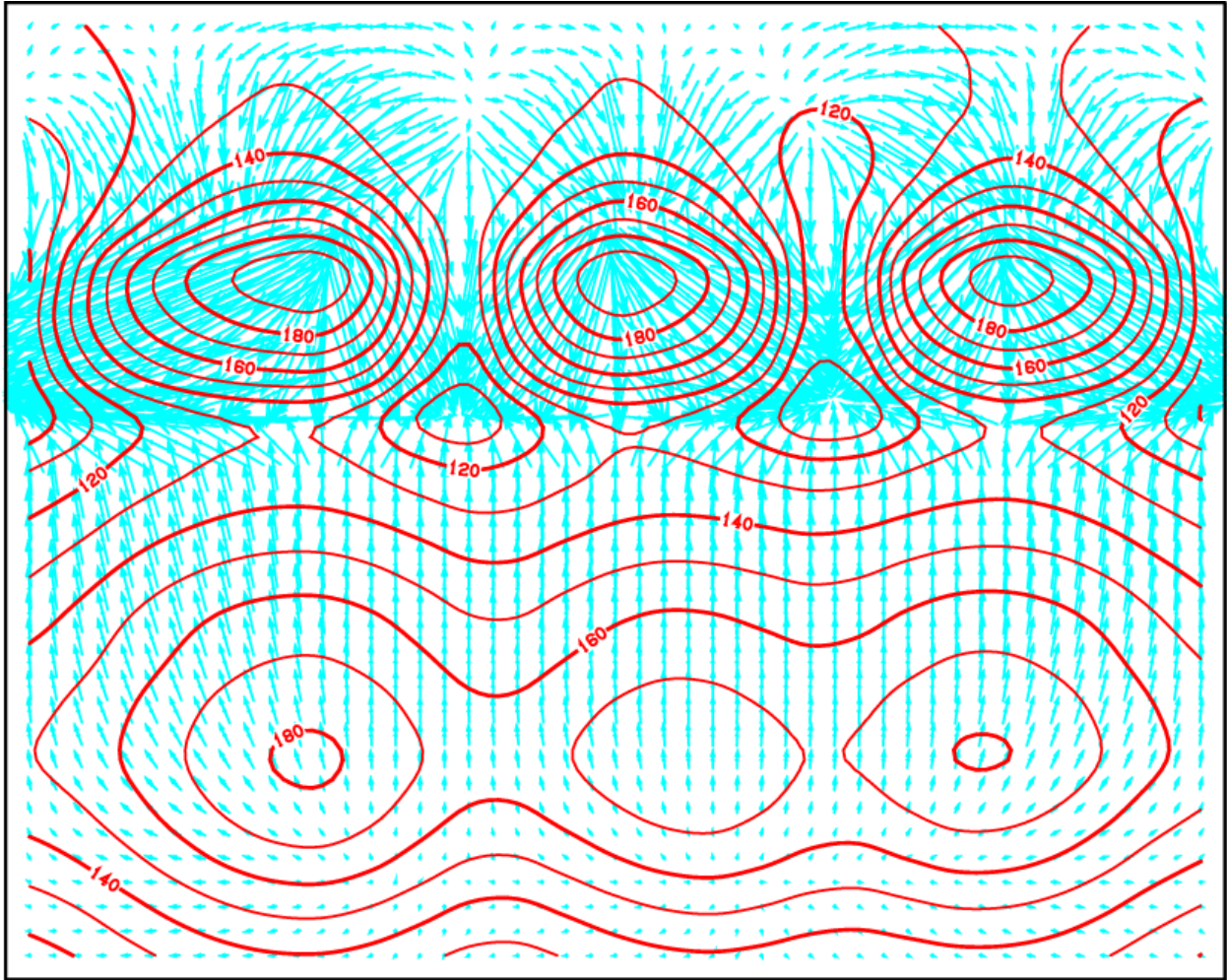


Figure 10n: Isotherms (red lines) and flow vectors (blue) in the horizontal x-y plane  $k=14$ .

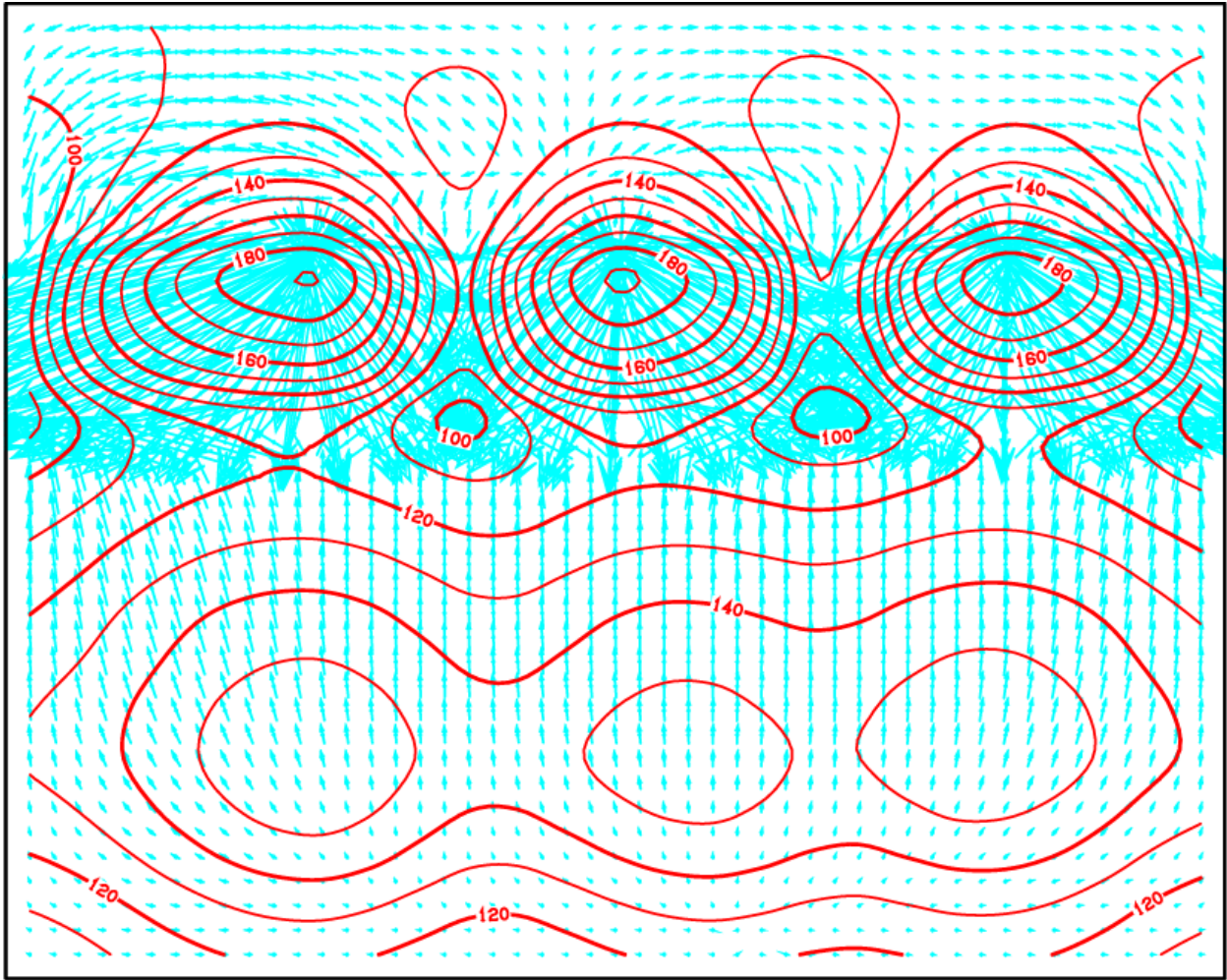


Figure 10o: Isotherms (red lines) and flow vectors (blue) in the horizontal x-y plane  $k=15$ .

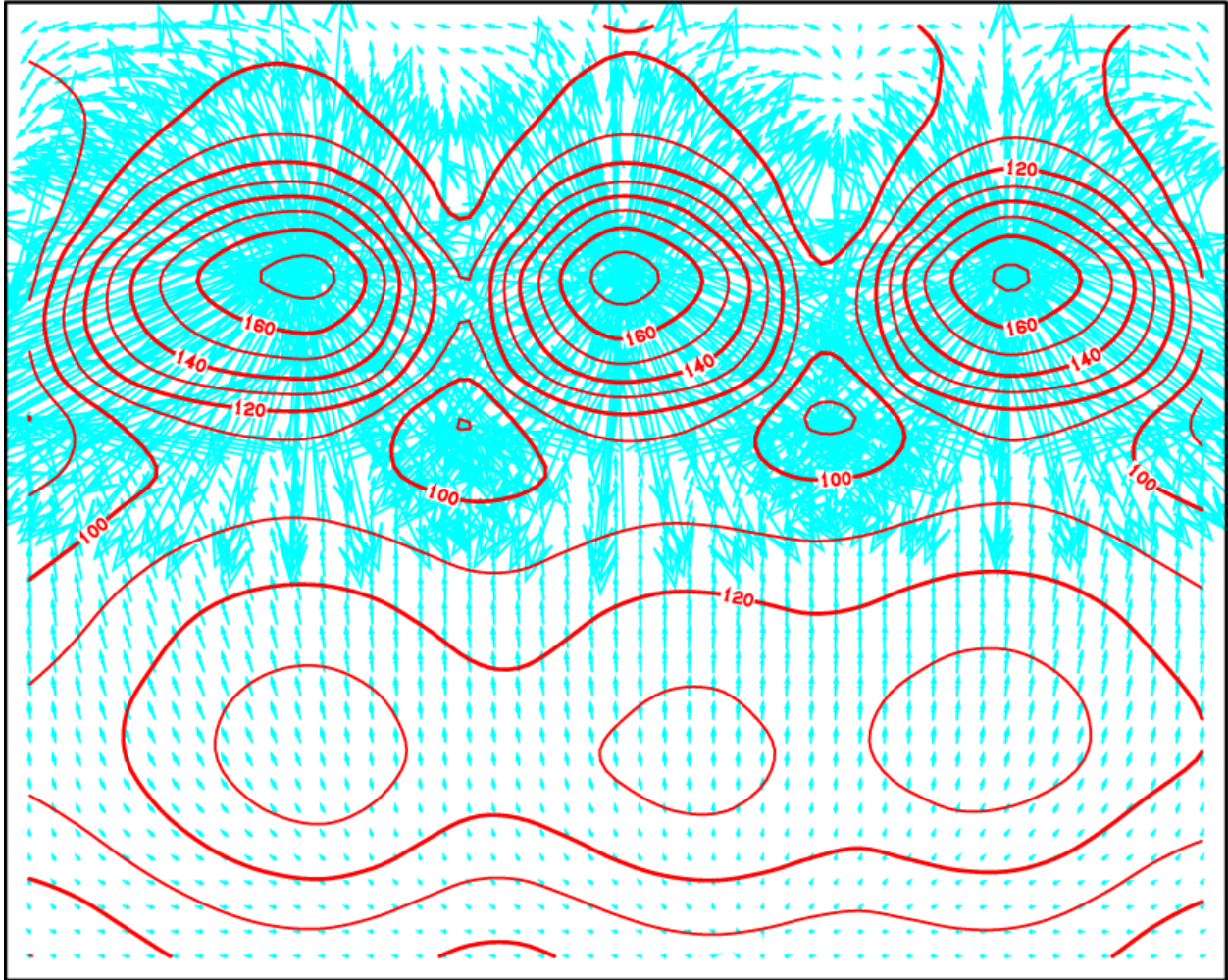


Figure 10p: Isotherms (red lines) and flow vectors (blue) in the horizontal x-y plane  $k=16$ .

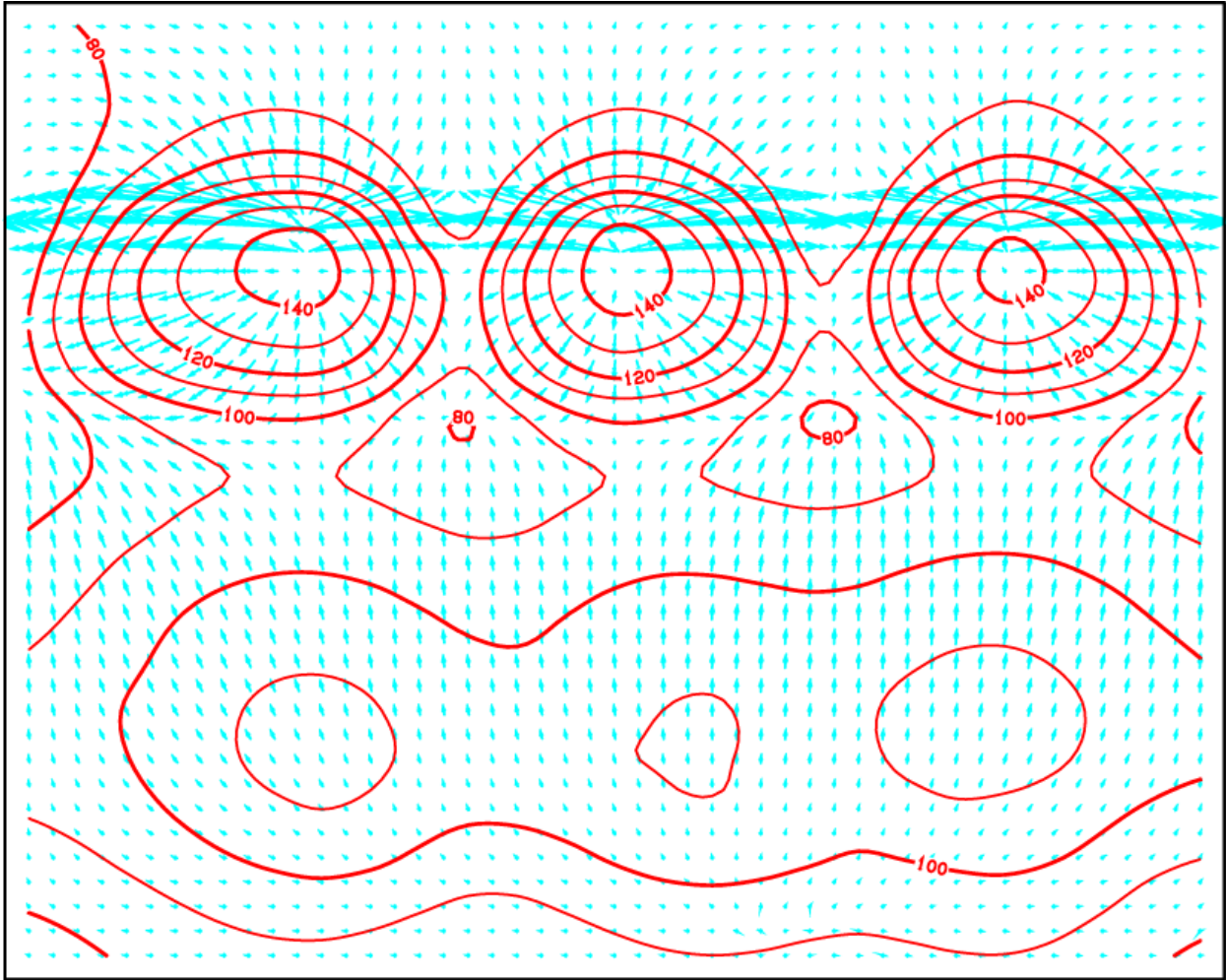


Figure 10q: Isotherms (red lines) and flow vectors (blue) in the horizontal x-y plane  $k=17$ .

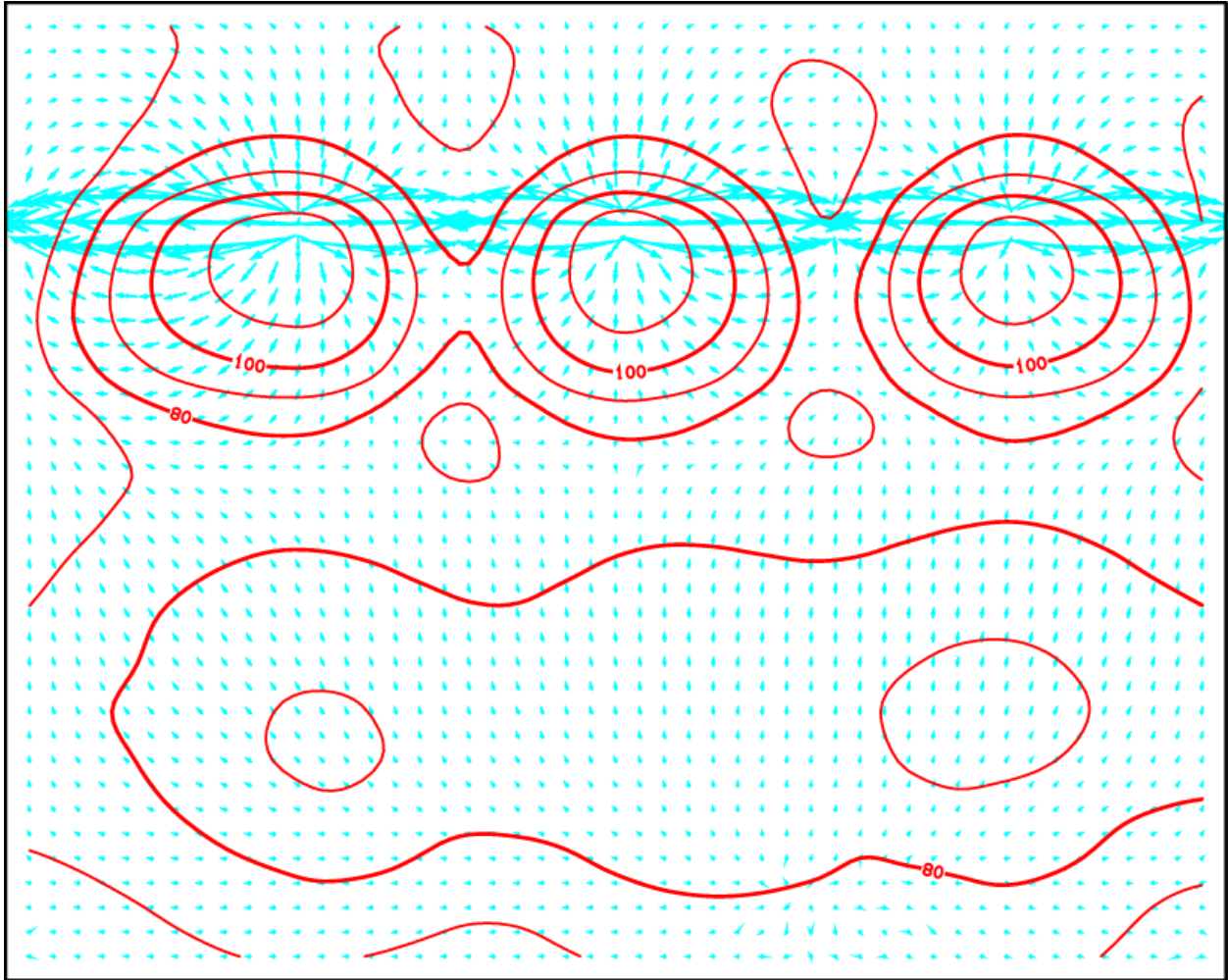


Figure 10r: Isotherms (red lines) and flow vectors (blue) in the horizontal x-y plane  $k=18$ .

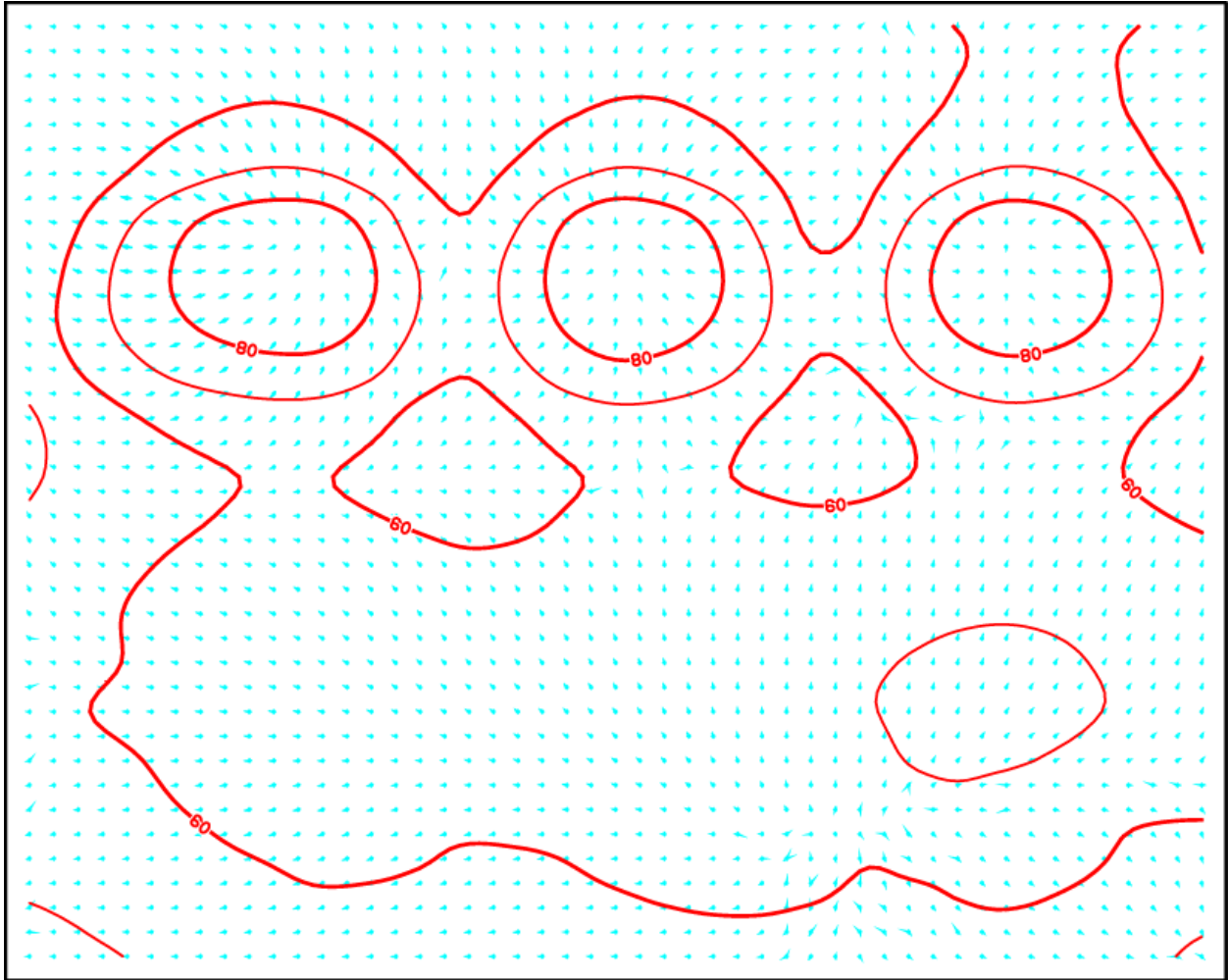


Figure 10s: Isotherms (red lines) and flow vectors (blue) in the horizontal x-y plane  $k=19$ .

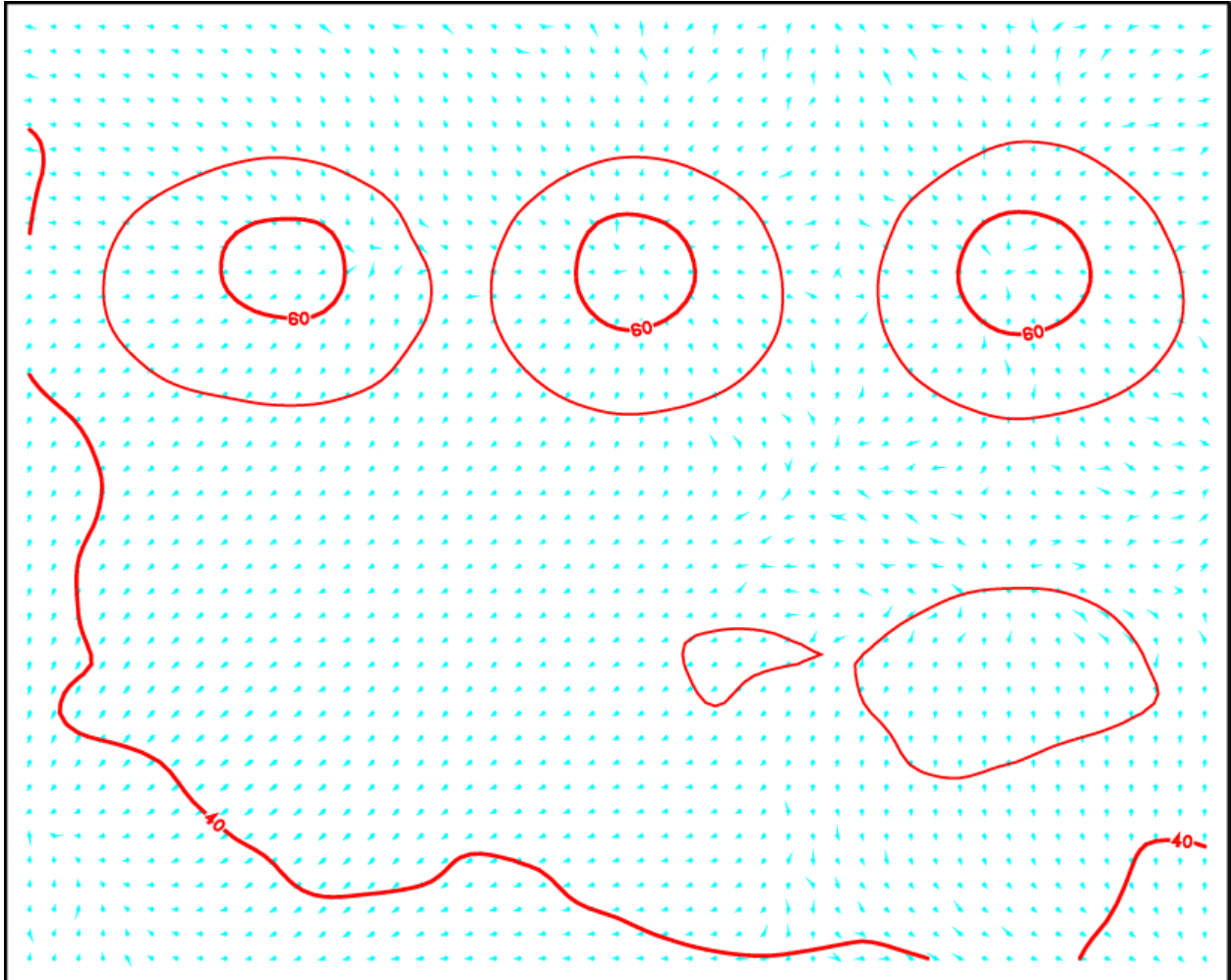


Figure 10t: Isotherms (red lines) and flow vectors (blue) in the horizontal x-y plane  $k=20$ .

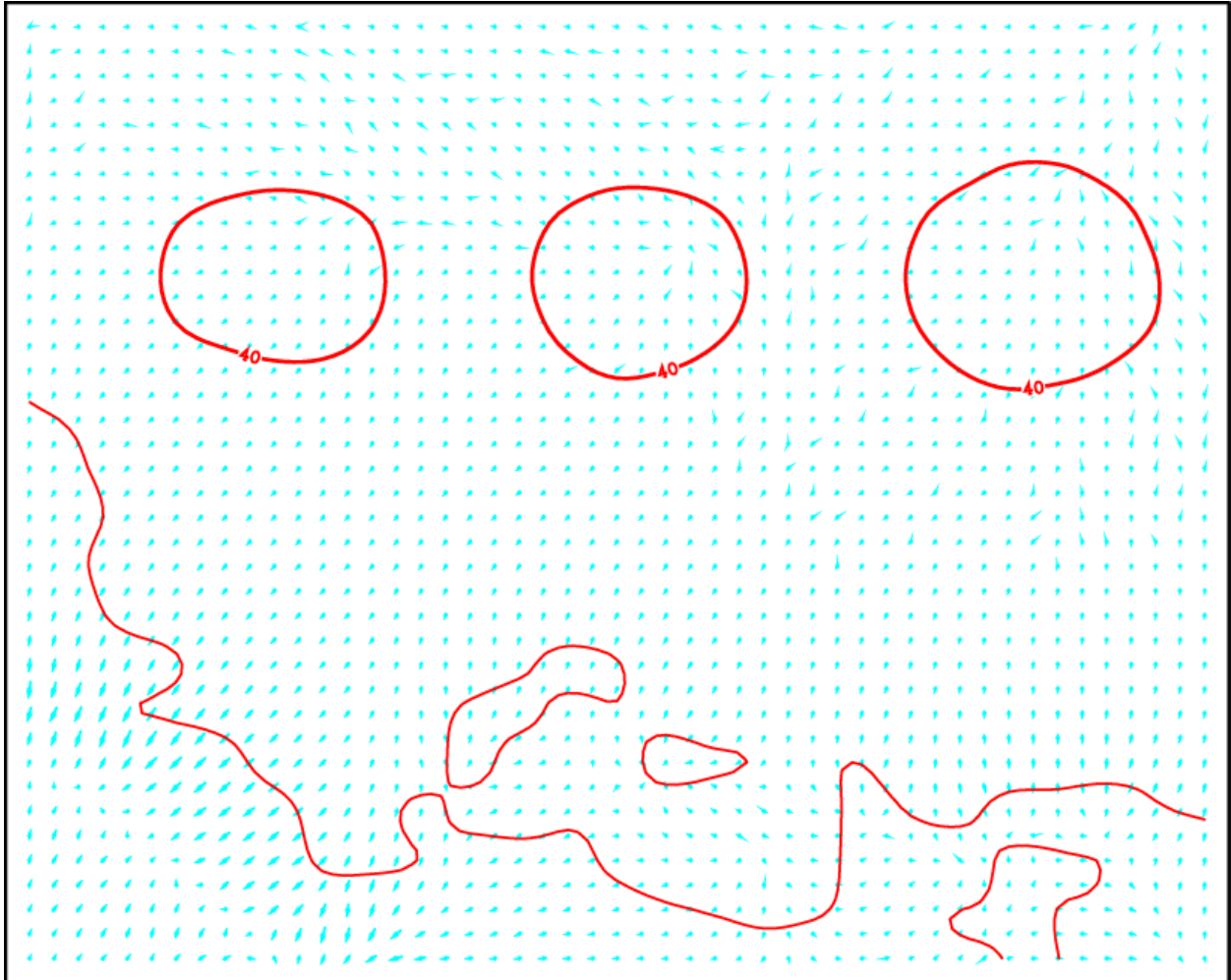


Figure 10u: Isotherms (red lines) and flow vectors (blue) in the horizontal x-y plane  $k=21$ .

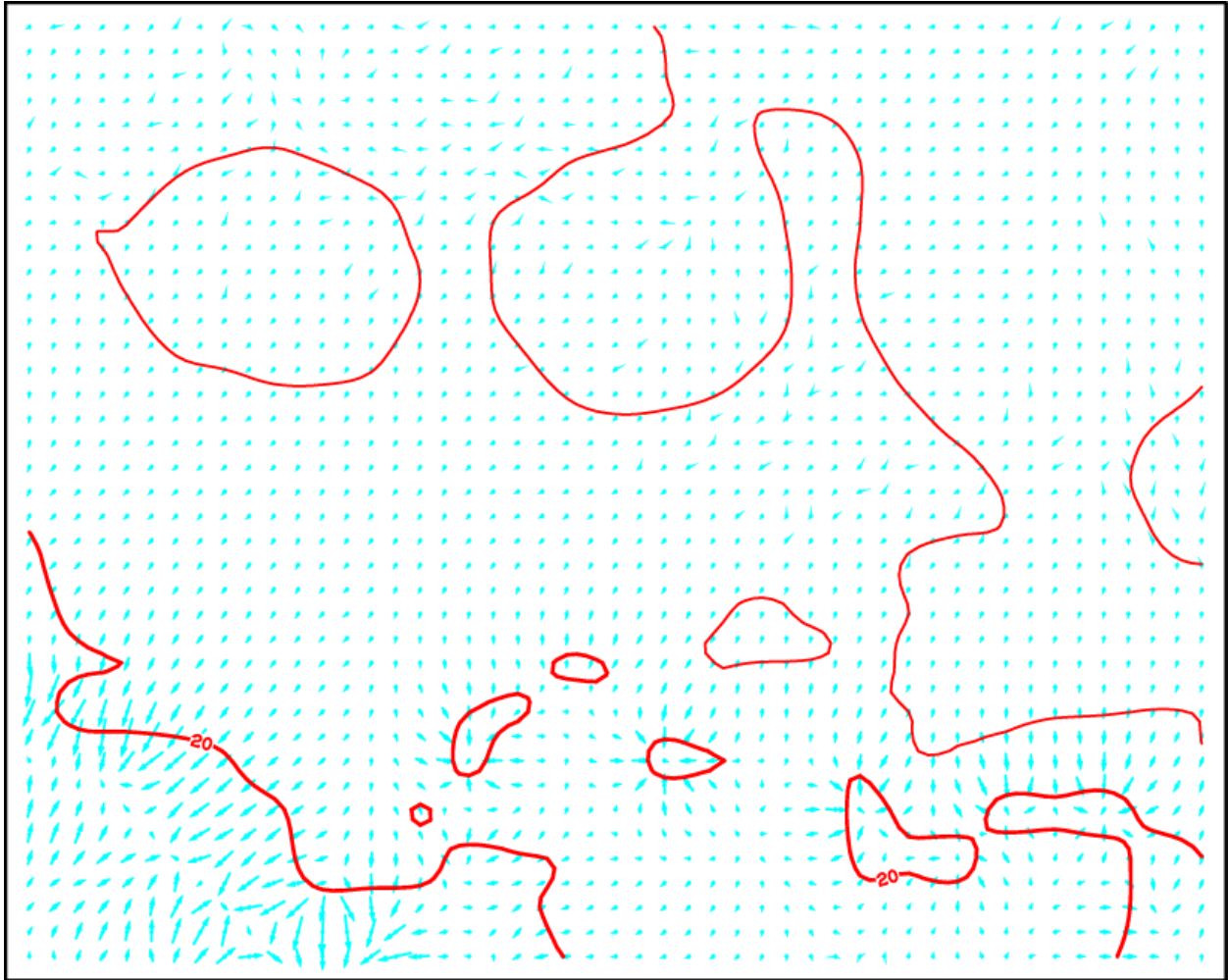


Figure 10v: Isotherms (red lines) and flow vectors (blue) in the horizontal x-y plane  $k=22$ .

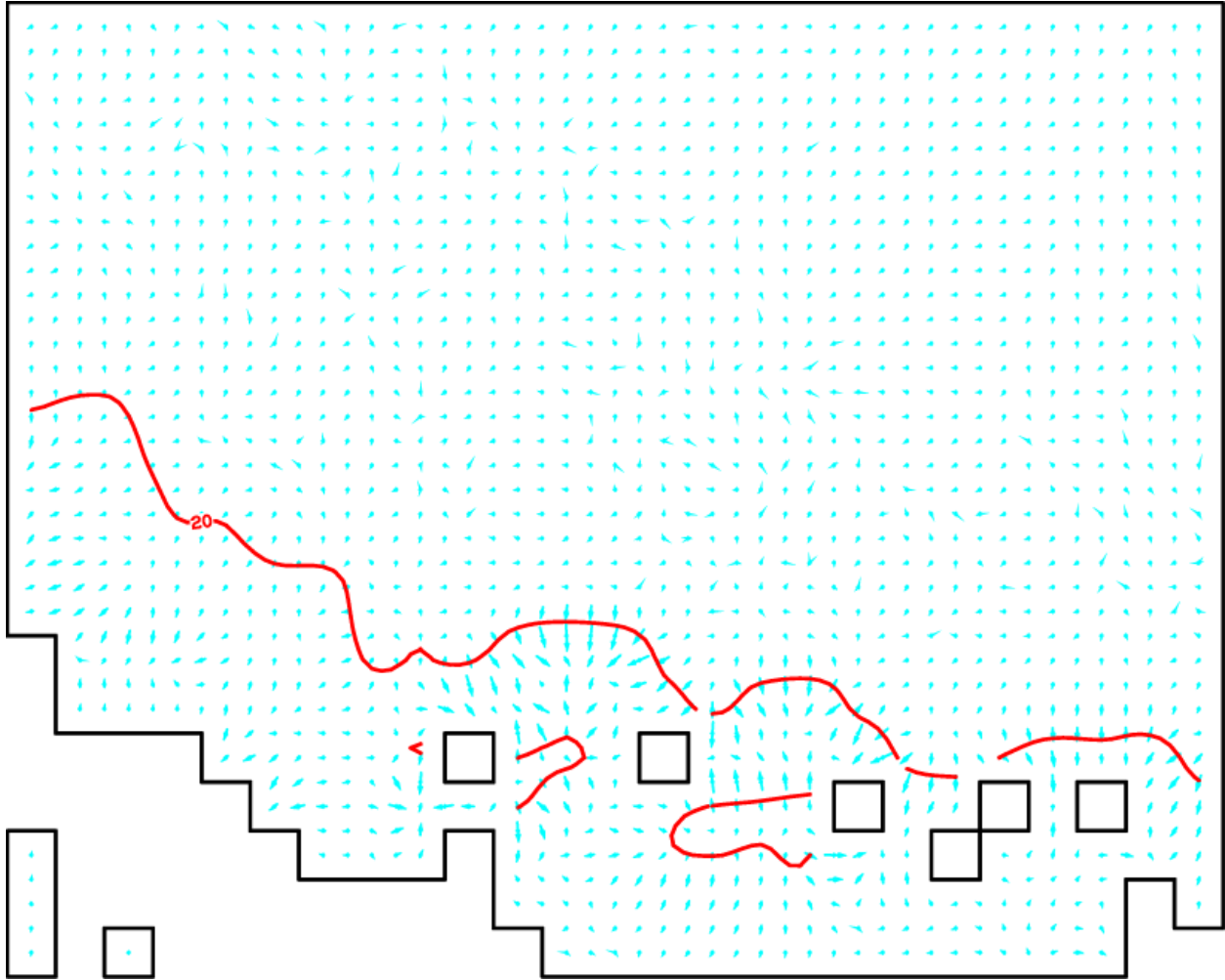


Figure 10w: Isotherms (red lines) and flow vectors (blue) in the horizontal x-y plane  $k=23$ . Some of the grid blocks in this layer are void.

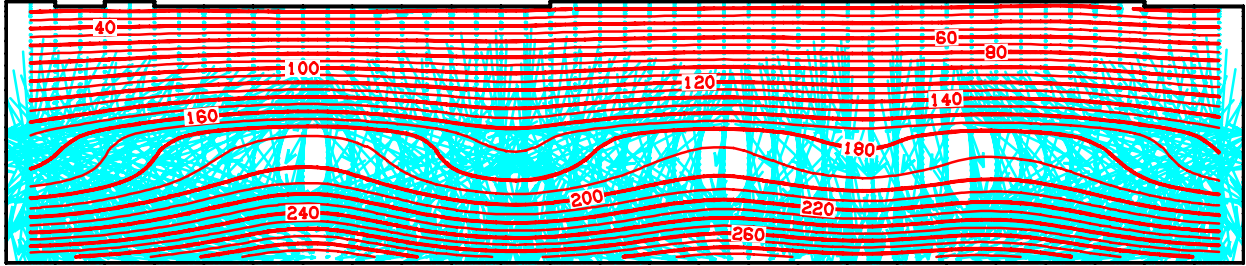


Figure 11a: Isotherms (red lines) and flow vectors (blue) in the vertical x-z plane  $j=1$ .

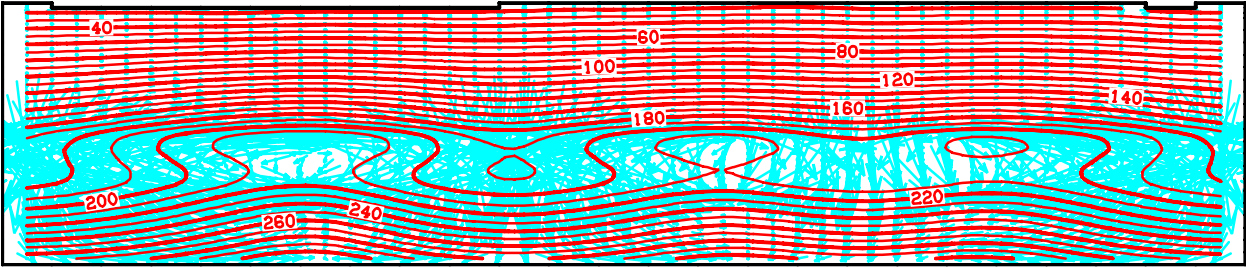


Figure 11b: Isotherms (red lines) and flow vectors (blue) in the vertical x-z plane  $j=2$ .

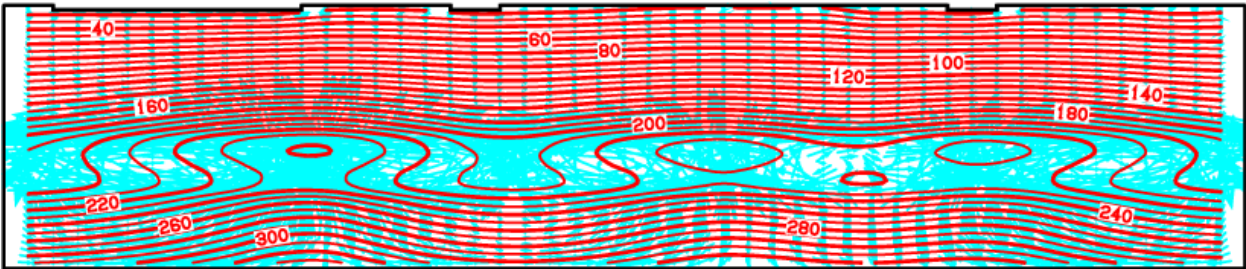


Figure 11c: Isotherms (red lines) and flow vectors (blue) in the vertical x-z plane  $j=3$ .

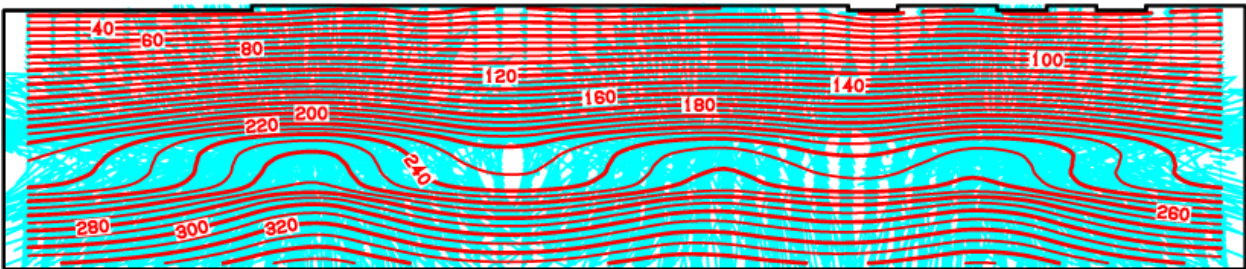


Figure 11d: Isotherms (red lines) and flow vectors (blue) in the vertical x-z plane  $j=4$ .

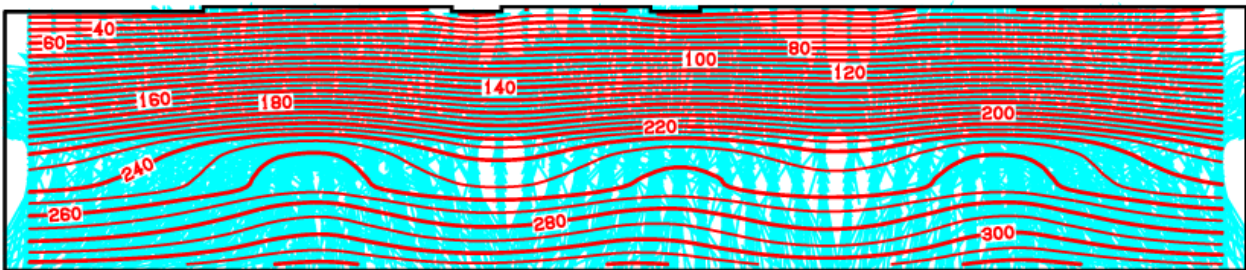


Figure 11e: Isotherms (red lines) and flow vectors (blue) in the vertical x-z plane  $j=5$ .

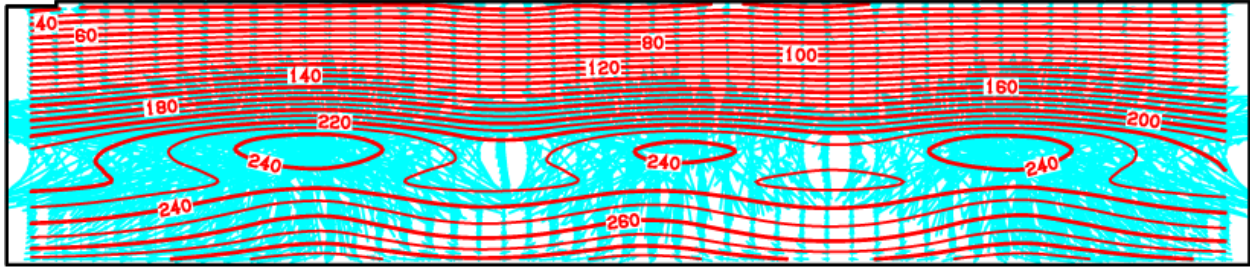


Figure 11f: Isotherms (red lines) and flow vectors (blue) in the vertical x-z plane  $j=6$ .

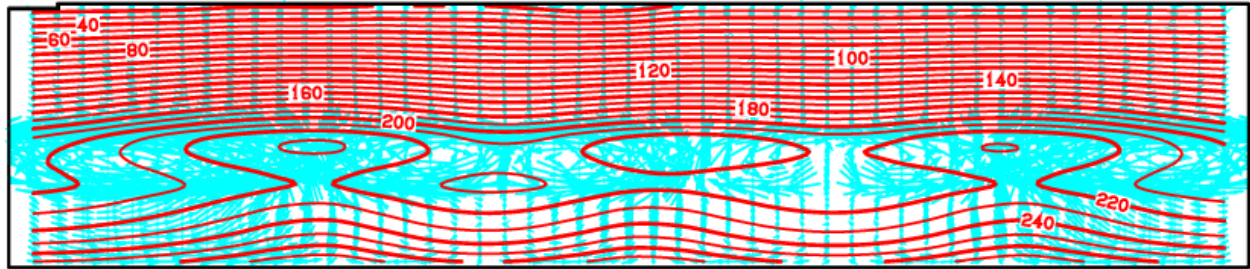


Figure 11g: Isotherms (red lines) and flow vectors (blue) in the vertical x-z plane  $j=7$ .

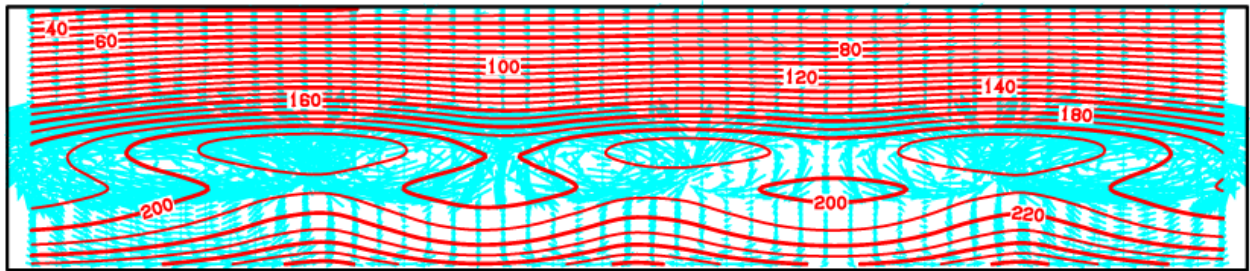


Figure 11h: Isotherms (red lines) and flow vectors (blue) in the vertical x-z plane  $j=8$ .

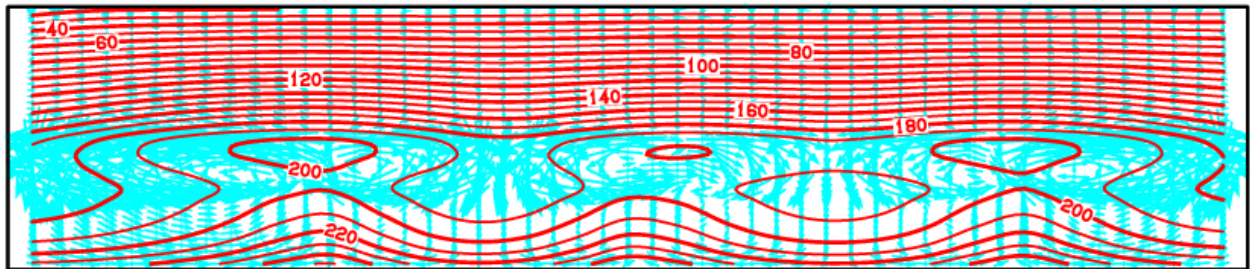


Figure 11i: Isotherms (red lines) and flow vectors (blue) in the vertical x-z plane  $j=9$ .

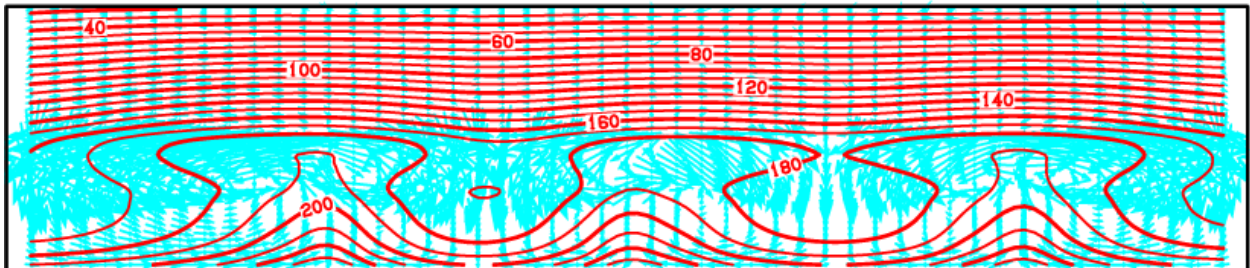


Figure 11j: Isotherms (red lines) and flow vectors (blue) in the vertical x-z plane  $j=10$ .

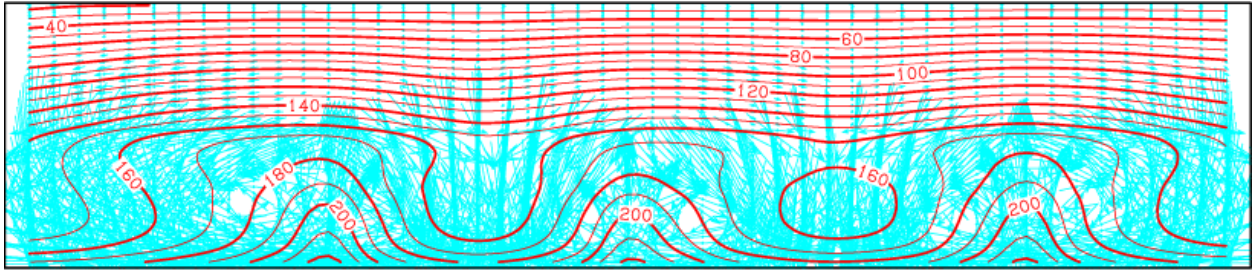


Figure 11k: Isotherms (red lines) and flow vectors (blue) in the vertical x-z plane  $j=11$ .

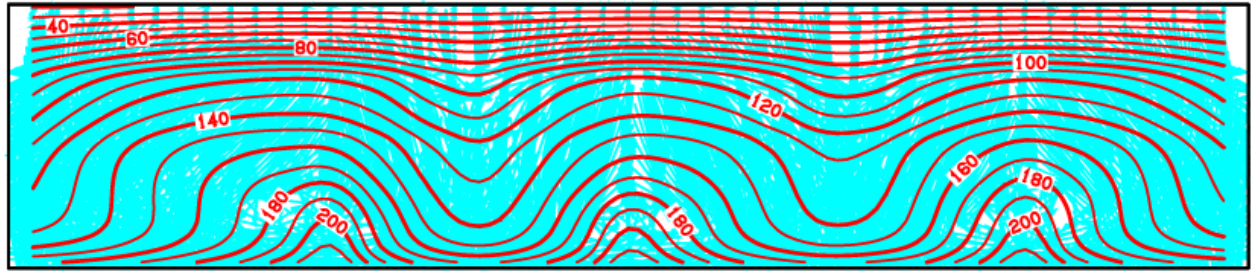


Figure 11l: Isotherms (red lines) and flow vectors (blue) in the vertical x-z plane  $j=12$ .

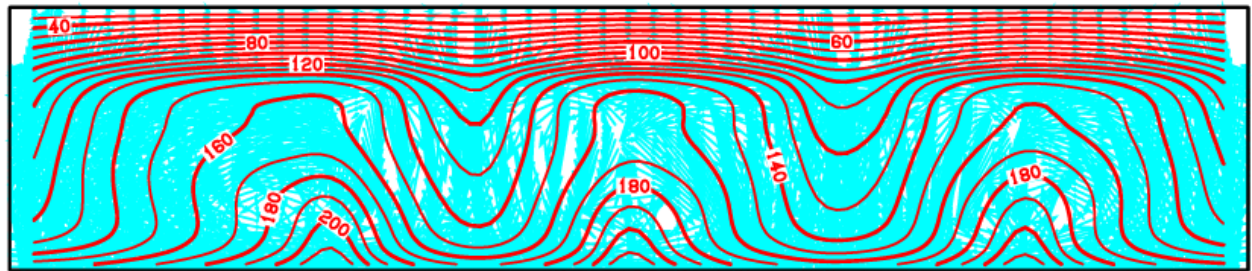


Figure 11m: Isotherms (red lines) and flow vectors (blue) in the vertical x-z plane  $j=13$ .

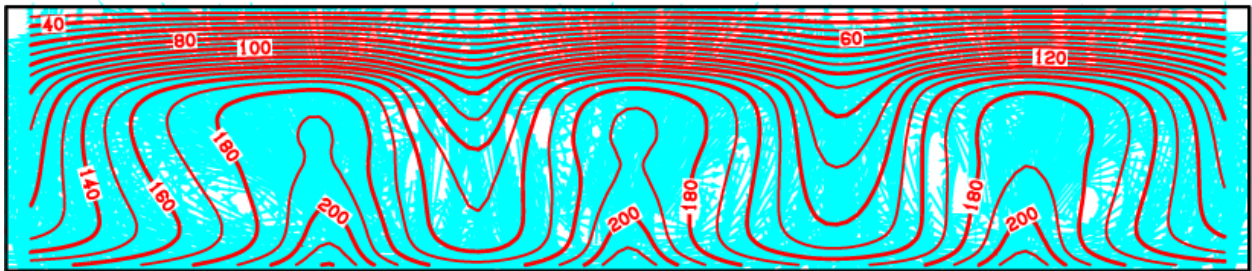


Figure 11n: Isotherms (red lines) and flow vectors (blue) in the vertical x-z plane  $j=14$ .

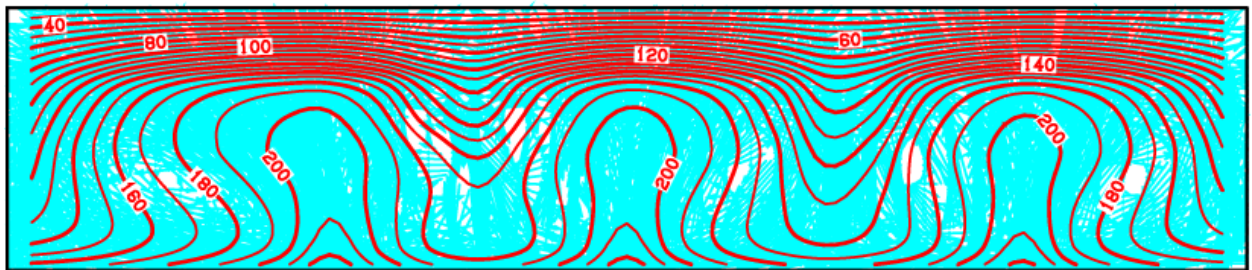


Figure 11o: Isotherms (red lines) and flow vectors (blue) in the vertical x-z plane  $j=15$ .

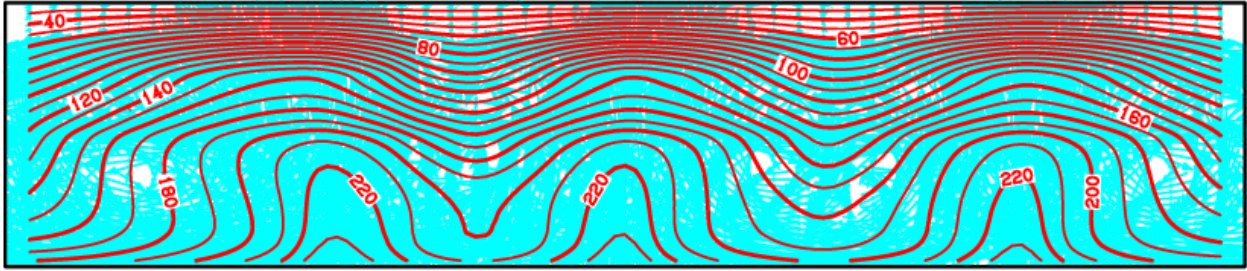


Figure 11p: Isotherms (red lines) and flow vectors (blue) in the vertical x-z plane  $j=16$ .

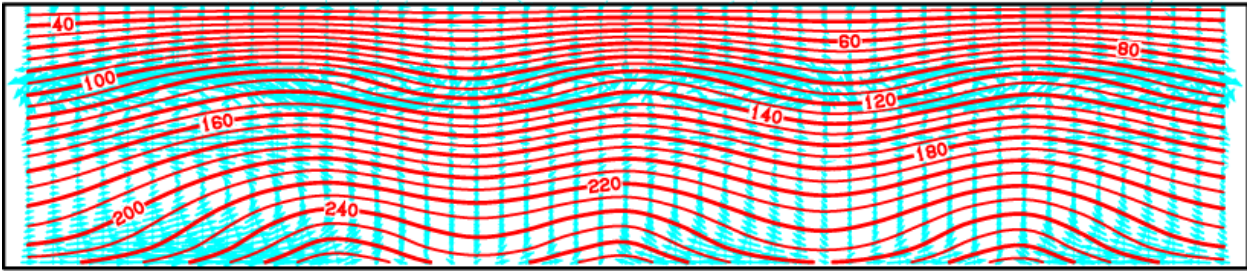


Figure 11q: Isotherms (red lines) and flow vectors (blue) in the vertical x-z plane  $j=17$ .

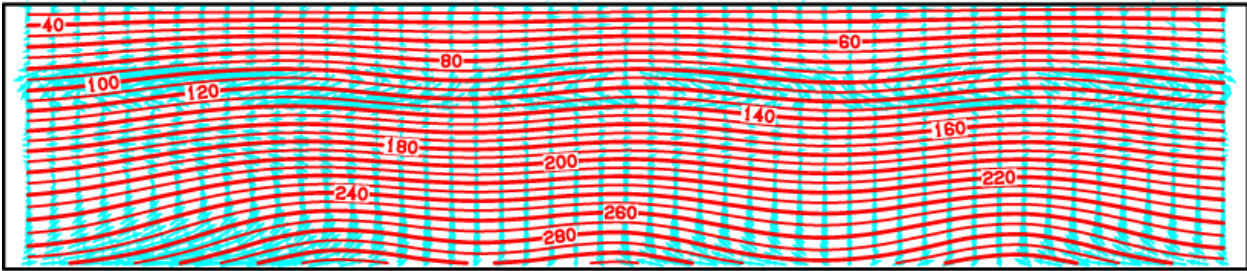


Figure 11r: Isotherms (red lines) and flow vectors (blue) in the vertical x-z plane  $j=18$ .

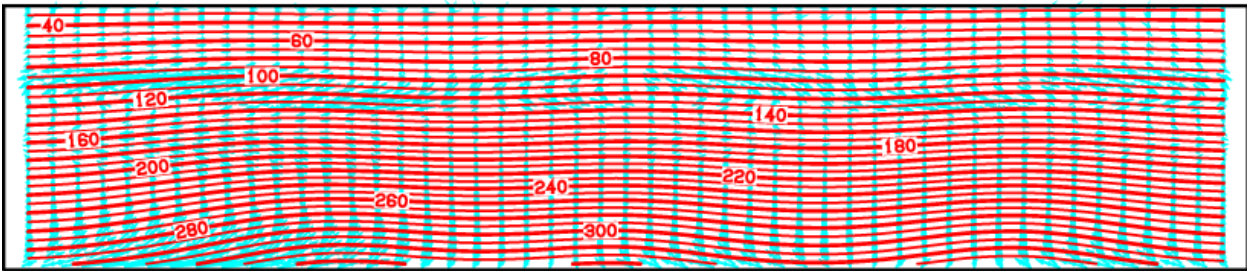


Figure 11s: Isotherms (red lines) and flow vectors (blue) in the vertical x-z plane  $j=19$ .

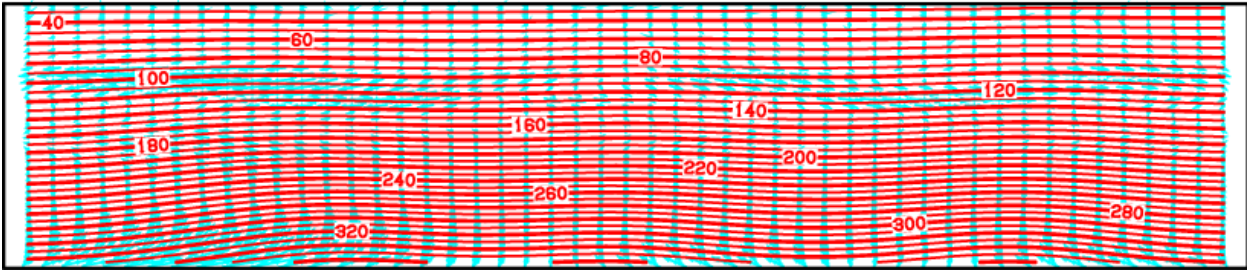


Figure 11t: Isotherms (red lines) and flow vectors (blue) in the vertical x-z plane  $j=20$ .

## **V. Future Work**

The preceding sections present a 3-D natural state model for the Mountain Home geothermal prospect. The latter model covers only a small part (about 6 %) of the area included in the regional model (Garg, 2015). The regional model was conditioned using the available temperature data from five (5) deep wells in the area, and incorporated a particularly simple representation of lithology. Since the regional model was developed, various geophysical surveys (gravity, magnetic, Magnetotelluric) surveys have been carried out in the area. Results from the gravity and MT surveys have provided important information on permeability distribution in the Mountain Home area. The current natural state model incorporates the latter information, and therefore provides a more accurate representation of the subsurface. At present, no pressure data are available, and it is not known if the computed pressures correspond to reality. Acquisition of reliable pressure data will require access to deep wells; such access is also required for well tests designed to measure subsurface permeability distribution. The model will no doubt evolve as additional data become available.

## **VI. References**

Garg, S.K. (2015), Mountain Home Geothermal Area: Preliminary Natural State Model, Technical Report, Leidos Inc., San Diego, California.

Glen, J.M.G., Liberty, L., Gasperikova, E., Siler, D., Shervais, J., Ritzinger, B., Athens, N., Earney, T. (2017), Geophysical Investigations and Structural Framework of Geothermal Systems in west and southcentral Idaho: Camas Prairie and Mountain Home, Proceedings 41<sup>st</sup> Workshop on Geothermal Reservoir Engineering, Stanford University, Stanford, California.

Pritchett, J.W. (2011), STAR User's Manual Version 11.0, Leidos Inc., San Diego, California.

